



HAL
open science

Messinian canyons morphology of the Rhône and Ardèche rivers (south-east France): new insights from seismic profiles

Damien Do Couto, Edward Marc Cushing, Ludovic Mocochain, Jean-Loup Rubino, Florian Miquelis, Franck Hanot, Berenice Froment, Celine Gelis, Hubert Camus, Nanaba Bagayoko, et al.

► To cite this version:

Damien Do Couto, Edward Marc Cushing, Ludovic Mocochain, Jean-Loup Rubino, Florian Miquelis, et al.. Messinian canyons morphology of the Rhône and Ardèche rivers (south-east France): new insights from seismic profiles. Bulletin de la Société Géologique de France, In press, Messinian Crisis, 10.1051/bsgf/2024015 . hal-04716686

HAL Id: hal-04716686

<https://hal.science/hal-04716686v1>

Submitted on 1 Oct 2024

HAL is a multi-disciplinary open access archive for the deposit and dissemination of scientific research documents, whether they are published or not. The documents may come from teaching and research institutions in France or abroad, or from public or private research centers.

L'archive ouverte pluridisciplinaire **HAL**, est destinée au dépôt et à la diffusion de documents scientifiques de niveau recherche, publiés ou non, émanant des établissements d'enseignement et de recherche français ou étrangers, des laboratoires publics ou privés.



Distributed under a Creative Commons Attribution 4.0 International License

1 **Messinian canyons morphology of the Rhône and Ardèche rivers (south-east**
2 **France): new insights from seismic profiles**

3

4 **Morphologie des canyons messiniens du Rhône et de l'Ardèche : apport de**
5 **nouveaux profils sismiques**

6

7 Damien Do Couto^{1*}, Edward Marc Cushing², Ludovic Mocochain¹, Jean-Loup Rubino¹,
8 Florian Miquelis³, Franck Hanot³, Bérénice Froment², Céline Gélis², Hubert Camus⁴, Nanaba
9 Bagayoko², Olivier Bellier⁵

10 *damien.do_couto@sorbonne-universite.fr

11 1: Sorbonne Université-Institut des Sciences de la Terre de Paris (ISTeP), UMR 7193, France

12 2: IRSN, Fontenay-aux-Roses, France

13 3: CDP Consulting, 7 boulevard Chanzy, Blois, 41000, France

14 4: CENOTE, 1 chemin de Valdegour, 30900, Nîmes

15 5: Aix Marseille Univ, CNRS, IRD, INRAE, Coll France, CEREGE, Aix-en-Provence, France

16 **Abstract**

17 Twelve available two-way time high-resolution seismic reflection profiles located in the central part
18 of the middle Rhône valley are interpreted. In addition, one of the profiles was reprocessed to
19 determine the P-wave velocities of the main geological units and to convert this profile into a depth
20 cross section. The Lower and Upper Cretaceous units are clearly identifiable on all the profiles, along
21 with the Messinian Erosion Surface (MES) carved out during the Messinian Salinity Crisis (MSC) by
22 the paleo-Rhône and its western tributaries, the Ardèche and Cèze paleo-canyons. The Plio-
23 Quaternary fill of these paleo-canyons shows at least 4 main units with an overall transgression. The
24 combination of geological data from geological maps, geological field surveys and borehole data
25 made it possible to model the MES in 3D at the scale of the region, and to produce depth/elevation
26 model. From a geological point of view, the interpretation of the seismic profiles enabled us to

27 reconstruct the stages in the sub-aquatic filling of the Messinian-Pliocene aggradation of the paleo-
28 river. Several Mass Transport Deposits (MTDs) were identified both during the drop and during the
29 rise in the Mediterranean Sea level. From a geomorphological point of view, this study provides new
30 insights in the route and longitudinal profile of paleo-rivers and, in particular, it deepens the profile
31 of the Paleo-Rhône at the latitude of the Tricastin region (up to 700 m b.s.l.) and significantly
32 modifies the course and depth of the Ardèche proposed in previous studies. The N-Ardèche river,
33 known to develop a karstic system during the MSC, is connected to a deep canyon, most likely
34 through a karstic pocket valley, as suggested by the very steep longitudinal profile of the MES.
35 Finally, from a structural point of view, our interpretation of the seismic profiles shows a broad ENE-
36 trending anticline structure associated with a normal fault which apparently did not affect the Mio-
37 Pliocene fill. In the southern part of the area, near the Uchaux anticline, the imaged structures
38 suggest the presence of a recent (syn- to post-Pliocene) fold propagation fault. In addition to all the
39 new information on the geology, morphology and methods of excavation and filling of the
40 Messinian paleo-canyon, the proposed topographic model of the paleo-canyon is crucial for
41 modelling seismic movement in the context of a basin with a complex geometry and, in particular,
42 for the numerical assessment of site effects in a context of low seismicity.

43 **Résumé**

44 12 profils de sismique-réflexion à haute résolution situés dans la partie centrale de la moyenne
45 vallée du Rhône ont été interprétés. Un des profils a été retraité pour déterminer les vitesses des
46 ondes P des principales unités géologiques et pour convertir cette ligne en une coupe en
47 profondeur. Sur tous ces profils, les unités du Crétacé inférieur et supérieur sont clairement
48 identifiables, de même que la surface d'érosion messinienne (MES) creusée pendant la crise de
49 salinité messinienne (CSM) par le paléo-Rhône et ses affluents de rive droite, les paléo-canyons de
50 l'Ardèche et de la Cèze. Le remplissage Plio-Quaternaire de ces paléo-canyons montre au moins 4
51 unités principales témoignant d'une transgression globale. La combinaison des données issues des
52 cartes géologiques, des études de terrain et des données de forages a permis de modéliser la MES à

53 l'échelle de la région. D'un point de vue géologique, l'interprétation des lignes sismiques a permis de
54 proposer une reconstruction des étapes du remplissage sub-aquatique de l'aggradation messino-
55 pliocène des paléo-rivières. Plusieurs épisodes de dépôts de transport de masse (MTD) ont été
56 interprétés comme résultant de différents cycles eustatiques. D'un point de vue
57 géomorphologique, cette étude fournit de nouvelles informations sur le tracé et le profil
58 longitudinal des paléo-rivières et, en particulier, elle approfondit le profil du Paléo-Rhône à la
59 latitude de la région du Tricastin (jusqu'à 700m sous le niveau de la mer) et modifie de manière
60 significative le cours et la profondeur de l'Ardèche tel qu'il a été proposé dans des études
61 antérieures. La Paléo-Ardèche, connue pour développer un système karstique pendant la MSC, est
62 connectée à un profond canyon, très probablement par le biais d'une reculée karstique, comme le
63 suggère le profil longitudinal très abrupt de la MES. Enfin, d'un point de vue structural,
64 l'interprétation des lignes sismiques montre une large structure anticlinale orientée ENE associée à
65 une faille normale d'extrados qui n'affecte apparemment pas le remplissage mio-pliocène. Dans la
66 partie sud de la zone, près de l'anticlinal d'Uchaux, les structures imagées suggèrent la présence de
67 failles ayant eu une activité récente (syn à post-pliocène) associée au rejeu de cet anticlinal. Les
68 nouvelles informations apportées par cette étude sur la géologie, la morphologie et les processus de
69 creusement et de remplissage du paléo-canyon messinien ont permis de proposer un modèle
70 topographique du paléo-canyon. Concernant l'évaluation de l'aléa sismique, l'utilisation d'un tel
71 modèle est cruciale pour modéliser les effets de site dans un bassin à géométrie complexe dans un
72 contexte de faible sismicité.

73 **Keywords** : Messinian Salinity Crisis, Messinian Erosional Surface, seismic profiles, Paleo-canyon,
74 Rhône, Ardèche.

75 **Mots-clés** : Crise de salinité messinienne, Surface d'érosion messinienne, profils sismique, paleo-
76 canyon, Rhône, Ardèche.

77 **1. Introduction**

78 In mainland France, the middle Rhône valley hosts a large number of energy-producing industries
79 and high-risk industries (nuclear power stations, hydroelectric dams, chemical factories, etc.). The
80 Tricastin region in the middle Rhône valley has been industrialised since the 1950s following the
81 construction of dam and major hydraulic works by the *Compagnie Nationale du Rhône* (Donzère-
82 Mondragon channel), then by nuclear fuel cycle facilities in the 1960s, and finally the Tricastin
83 nuclear power plant (cooled by channel water) in the 1970s. Even though south-east France is
84 known to be impacted by low to moderate seismicity (Ritz et al., 2021), rare yet powerful
85 earthquakes could occur in the study area, as shown by the Le Teil earthquake (~5 Mw) and shallow
86 earthquake swarms in Tricastin (~4-4.5 Mw; e.g. 1773, 1873, 1936; Thouvenot et al., 2009;
87 Manchuel et al., 2018; Bollinger et al., 2021). In addition, the region shows ancient surface ruptures
88 (paleoseismic) identified on the Nîmes Fault, the Ventoux Lure thrust and the La Rouvière Fault (Ritz
89 et al., 2021, Bellier et al., 2021), evidence for its past and probably significant seismic activity (Fig. 1).

90 The Le Teil earthquake, which occurred in November 2019 on the La Rouvière Fault (belonging to
91 the Cévennes Fault system) just north of the Tricastin area (Ritz et al., 2020, 2021) shed light on the
92 seismic hazard due to seismic amplification because of the presence of soft sediments in the Rhône
93 valley (Gélis et al., 2022), just below the nuclear facilities. The soft sediments are mostly made of
94 Pliocene deposits infilling a canyon carved by the paleo-Rhône during the Messinian Salinity Crisis
95 (Hsü et al., 1973; Clauzon, 1982), a recent (< 6 Ma) environmental crisis in which the Mediterranean
96 Sea level fell hundreds of metres below its present-day level. During this short episode (< 600 kyr)
97 the paleo-Rhône incised a canyon, but the present-day morphology in the area remains elusive as no
98 geophysical subsurface imaging enabled the production of a comprehensive 3D architecture.
99 Modelling of site effects (seismic amplification) requires a 3D image of the canyon that is as accurate
100 as possible, as well as information concerning the nature and thickness of the sedimentary fill
101 (Froment et al., 2022).

102 In the middle Rhône valley, the Tricastin area is also known to be the locus of a slope break (known
103 as a knickpoint) in the course of this Messinian Rhône canyon (Clauzon, 1982) that is hypothesised
104 to mark a stagnation phase during the sea-level drop caused by the Messinian Salinity Crisis
105 (Beaudoin *et al.*, 1997). Evidence of this knickpoint in the paleo-river profile was mainly based on
106 the Pierrelatte borehole that cross cut the base of the Pliocene (Ballesio, 1972). Although erosion
107 modelling along the whole Messinian paleo-Rhône reproduced a slope break in the same area, it did
108 not reproduce such an abrupt slope break but estimated a rather smoother transition from the
109 upstream paleo-Rhône to the downstream part (Gargani, 2004a). Detailed analysis of seismic
110 profiles would greatly improve our knowledge concerning the existence of this knickpoint.

111 In this study, we used surface data (geological maps, digital elevation model) and subsurface data
112 (seismic profiles, borehole data) to conduct a thorough analysis and to produce a 3D reconstruction
113 of the canyon morphology of the Messinian paleo-Rhône and its SW tributaries (paleo-Ardèche and
114 paleo-Cèze rivers). This paper considerably improves our knowledge of the processes by which the
115 canyon was dug and then filled in, in relation to the different stages of the Messinian salinity crisis.
116 Although to a lesser extent, our study also advances our knowledge of seismic hazards, e.g.
117 amplification of the seismic ground motion linked to the specific geological context, identification of
118 any active faults that could affect the plio-quadernary filling of the canyon, which is essential in a
119 context where critical industrial sites are present.

120 Here, we present the results of our analysis of high-resolution seismic profiles of the central part of
121 the middle Rhône valley. Analysis of the seismic profiles revealed details of the Messinian erosion
122 surface and the Pliocene filling of the Rhône, Ardèche and Cèze canyons. As part of this analysis, we
123 also wanted to link the stages of sub-aquatic filling, which are clearly visible on the profiles, to those
124 of the Messinian-Pliocene evolution of the aggradation of the paleo-river/river. Finally, we consider
125 the possible connection between the Ardèche Messinian canyon and its Messinian deep karst.

126 The rest of the paper is organised as follows: after presenting a synthesis of the regional geological
127 framework and describing the data used in this study, we conducted a cross-correlation of wells by
128 revisiting data collected from old and recent boreholes we then used together with seismic
129 interpretation to unravel the history of the Messinian-Pliocene history and to model the MES.
130 Finally, we discuss the results of this work with respect to the course and morphology of the Rhône
131 and Ardèche canyons, as well as their infill and structural geology.

132 **2 Geological framework**

133 ***2.1 Tectonic and stratigraphic framework***

134 The study area is located in mainland France in the middle Rhône valley (Fig. 1). It lies between the
135 Massif Central to the west and the Alps to the east. The Rhône flows from the inner Alps, through
136 the Jura fold belt and finally into the Tertiary basins formed during the extensions linked to the
137 opening of the West European Rift and the Gulf of Lions (Eocene, Oligocene). To the south, the
138 Rhône river flows into the Mediterranean Sea.

139 The Rhône plain is currently covered by Quaternary sediments (in grey in Figure 2). The right bank of
140 the Rhône mostly is composed of Lower and Upper Cretaceous series, while Miocene series cover
141 Saint-Resitut hill on the left bank of the river (Figure 2). Pliocene deposits (in pink in Figure 2) are
142 found on both sides of the Rhône river, mostly nested within Cretaceous series. After the Mesozoic
143 Tethysian rifting responsible for the inception of the major NE trending faults (Bonijoly *et al.*, 1996),
144 the study area experienced three main tectonic stages, namely (i) the Pyrenean shortening from
145 Paleocene to early Oligocene, (ii) the Oligocene-Early Miocene extension and (iii) the Miocene
146 Alpine shortening.

147 The convergence between the Iberian and Eurasian plate from the Paleocene to the early Oligocene
148 caused E-W oriented folds sometimes combined into N-verging thrusts that affected the Mesozoic
149 series (Arthaud and Laurent, 1995; Rangin *et al.*, 2010) as well as the reactivation of pre-existing NE-

150 striking faults in a left-lateral movements (Arthaud and Matte, 1975) such as the Nîmes fault. The
151 most prominent structures in the study area that resulted from this event are the Mondragon and
152 Orange anticlines to the southeast, the Echavarelles anticline in the centre of the study area, and
153 the Donzère anticline to the north (Fig. 2). From the Late Oligocene to the Early Miocene, the study
154 area experienced two successive E-W extensions related to the West-European rifting, followed by a
155 NW-SE extension concomitant with the opening of the Gulf of Lions and the rotation of the Corsica-
156 Sardinia blocks (Séranne *et al.*, 1995; Lacombe and Jolivet, 2005; Séranne *et al.*, 2021). These riftings
157 resulted in the inception or re-activation of NE-trending normal faults, most of which occurred
158 south-east of the study area (Ballas *et al.*, 2014). It has been reported that the Saint-Remèze fault
159 system may have been re-activated at that time, causing normal displacement along the fault
160 (Pascal *et al.*, 1989). More recent Alpine orogeny had little impact on the study area (Champion *et*
161 *al.*, 2000) as it mostly accommodated the deformation along major accidents further south, such as
162 the Luberon thrust (Rangin *et al.*, 2010; Clauzon *et al.*, 2011), and along the northern part of NE-SW
163 Cevennes-fault system (Bellier and Vergely, 1987). Vertical movements are also documented. The
164 alpine forebulge uplift (Besson, 2005) was mainly active during the Lower and Middle Miocene and
165 partially explains how in some reliefs, for example, in the Saint Restitut Hill, Upper Miocene
166 conglomerates remain over Burdigalian strata. Based on numerical modelling of isostatic responses
167 of the Rhône valley during the MSC, Gargani (2004a) evaluated a positive rebound of between 20
168 and 180 m, in agreement with the results of field studies (Mocochain *et al.*, 2006b). Other post-
169 alpine movements created a slight uplift and tilting of the Miocene, Pliocene and even Quaternary
170 series have already been reported by other authors (Guérin, 1973; Besson, 2005). This deformation
171 results from post alpine isostatic adjustment (due to erosion unloading; Malcles *et al.*, 2020) or is
172 linked to the uplift of the neighbouring Massif Central (Olivetti *et al.*, 2016).

173 The general structural trend in the study area is characterised by an overall gentle monoclinial trend,
174 slowly dipping east-south-eastwards. However, within the Rhône valley, there is an outcrop of
175 Barremian limestone of Urgonian facies in the city of Pierrelatte. The Urgonian is also recorded at a
176 depth of 339 m (283 m b.s.l.) in the Pierrelatte well. To explain the rapid offset of Urgonian rocks,

177 Debelmas *et al.* (2004) suggested the occurrence of downfaulting across a NE-trending structure
178 known as the Pierrelatte fault. So far, data proving its existence at depth and its geometry are
179 lacking.

180 Figure 3 shows a stratigraphic column of the whole study area based on Champenois *et al.*, (1971),
181 Masse *et al.*, (1980), Pascal *et al.* (1989) and Debelmas *et al.*, (2004). It starts from the Hauterivian
182 marl and limestone that can vary in thickness from 50 to 750 m (Pascal *et al.*, 1989). As detailed
183 later, this formation was not distinguished on the seismic reflection image, so only its top is
184 indicated on the lithostratigraphic log. The most prominent and thickest carbonate strata outcrop in
185 the Saint Remèze plateau and along the Ardèche Gorges (Ferry & Rubino, 1989): they are made of
186 ammonite- and rudist-rich limestone of Barremian-Lower Aptian age known as the Urgonian facies,
187 and are approximately 550-600 m thick. Locally, the thickness of the Barremian can exceed 700 m,
188 as recorded in the Mondragon well considering the local dip of layers (BSS002CLTG in the borehole
189 subsurface database BSS from BRGM: <https://infoterre.brgm.fr>). The Urgonian terminates by a mid-
190 Aptian marl and limestone succession known locally as the Bedoulian facies (Fig. 3) belonging to the
191 Chabert formation (Pictet & Delanoye 2017). The Aptian ends with ~100 m of dark grey marls and
192 glauconite bearing sandy limestone, known locally as the Gargasian-Clansayesian sandstones facies.
193 The Albian mainly comprises sandstone/calcareous sandstones and marls, about 80-90 m thick,
194 topped by the uppermost Albian Marls (Vraconian flooding). The Cenomanian evolves from lignites
195 and sandstones (quartzarenites) to the south and southeast of the study area (Uchaux area;
196 Malartre, 1994), towards marly limestone intercalated with calcareous sandstones in the northeast
197 (Clansayes area, Fig. 2). The stratigraphic column continues with ~200 to 250-m thick glauconitic
198 sandstones, as well as sandy to micritic limestones Turonian in age, outcropping in the Mondragon
199 anticline (Fig. 2). The Upper Cretaceous then evolves into Coniacian sandy limestones, whose
200 thickness ranges from 30 to ~150 m and grades into Santonian sandstones with rudist intercalations.
201 The Upper Cretaceous is unconformably overlain by Eocene and then Oligocene deposits. The
202 Eocene is marked by red and white lateritic sands and quartz sandstones, often found as lenses tens

203 of metres wide. At its base, the Oligocene is also marked by an unconformity, which mainly outcrops
204 on the northeastern side of the study area, and mostly comprises lacustrine deposits, sometimes
205 brackish, composed of marls and limestones evolving into red marls towards the top of the series.
206 As a whole, the Oligocene is ~50 to 70 m thick and dips slightly towards the E-SE.

207 The Miocene is unconformably deposited above previous series. In our study area, the Miocene
208 mainly consists of marine Burdigalian strata in Saint-Restitut hill, made of approximately 120 m thick
209 molasses (conglomerates, sandstones evolving to marls and carbonates, partly bioclastic at the top
210 of the series; Lesueur et al. 1990). It outcrops at an altitude of approximately 180 m on the western
211 side of Saint-Restitut hill, with a mean 3° dip towards the E-SE. Younger Miocene series, Langhian to
212 Messinian in age, outcrop further east of the study area in the Miocene Valréas Basin (Demarcq,
213 1970; Rubino et al., 1990), as well as further south fringing the Mondragon anticline (Fig. 2).

214 The Pliocene is unconformably nested within earlier series, mostly in contact with Cretaceous strata
215 (Fig.2). Because Pliocene series infill Messinian valleys and canyons, its thickness varies markedly
216 from one place to another. Thanks to descriptions of both outcrops and boreholes like the
217 Pierrelatte well (Fig. 4), the Pliocene in the Tricastin area is known to be made up of four subunits
218 (Ballesio, 1972), from the base to the top:

219 - basal pebble-sized conglomerates reworking lower Miocene material, and lenticular breccia bodies
220 lying on top of slopes reworking hillside strata such as Miocene deposits; the thickness of this
221 subunit can reach 50 m locally

222 - continental fluviolacustrine deposits made of variegated marls followed by azoic greyish to
223 yellowish clays/marls and topped by brackish layers containing bivalves (such as in Saint-Marcel
224 d'Ardèche)

225 - marine bluish to greyish marls/clays with a small proportion of sand, locally containing coastal
226 fauna (Cerithium and Pectinidae species)

227 – fluvio-lacustrine sands, conglomerates and marls, exhibiting some lignite layers and containing
228 freshwater fauna.

229 On top of this succession lie unconformably Quaternary terraces (Mandier, 1989), however these
230 are not dated.

231

232 **2.2 The Messinian Salinity Crisis in the Rhône Valley**

233 The Messinian Salinity Crisis is an outstanding paleo-environmental event characterised by a two-
234 stage sea-level fall (Clauzon *et al.*, 1996) followed by a two-stage sea-level rise (Bache *et al.*, 2012;
235 review in Roveri *et al.*, 2014). The first sea-level drop, occurring at 5.97 Ma (Manzi *et al.*, 2013) was
236 moderate in amplitude (150-200m in Clauzon *et al.*, 2015b), it was responsible for the precipitation
237 of evaporites in the peripheral shallow basin around the Mediterranean Sea. At the end of the
238 Messinian period, at 5.6 Ma (CIESM, 2008), a huge drop in the sea level of the Mediterranean Sea
239 estimated at between 800 and 1,500 m (Bache *et al.*, 2009, Urgeles *et al.*, 2011) led to the incision of
240 deep canyons such as the Rhône canyon, down to 1,300 m below present-day sea level (Guennoc *et*
241 *al.*, 2000) and to more than 1,000 m below the Camargue (Clauzon, 1982; Clauzon *et al.*, 1992).
242 Reflooding following the drawdown took place in two stages, with a first slow sea-level rise,
243 followed at 5.46 Ma by a rapid sea-level rise (Bache *et al.*, 2012). Sea-level oscillations during the
244 MSC also led to the development of a karstic network along the Ardèche river (Mocochain *et al.*,
245 2006b, 2009).

246 The incision resulting from the fall in the level of the Mediterranean Sea is highlighted by the deeply
247 unconformable nature of the Pliocene series over all the preceding formations. Along the Rhône
248 valley, this specific unconformity has been known since the pioneer work of Fontannes (1882), see
249 Clauzon (1974) for a historical review. Previously, the estimated incision depth in our study area was
250 based on (1) the identification of a pre-evaporitic abandonment surface (i.e. the last and topmost

251 gently dipping surface of the upper Miocene alluvial plain), which recorded the position of the
252 Rhône just before the MSC (i.e. at an altitude of 360 m on the Saint-Remèze plateau; Clauzon, 1982,
253 Martini, 2005, 2022), and (2) the interpretation of the Pierrelatte well (Demarcq, 1960) suggesting
254 that the base of Pliocene was located at -236 m below present sea-level (b.s.l). These observations
255 allowed Clauzon (1982) to estimate the depth of incision at 580 m in the Tricastin area. Clauzon
256 (1982) also drew the Messinian Rhône canyon profile, based on a compilation of wells that crossed
257 the base of Pliocene deposits, highlighting the occurrence of a knickpoint south of the Tricastin area.
258 North of this knickpoint, the Messinian Rhône appeared to have an average slope of $\sim 1.8^\circ$ ($\sim 3\%$),
259 which increased southwards with an average slope of $\sim 9^\circ$ ($\sim 16\%$).

260 The question of the junction between the Ardèche valley and the Messinian Rhône canyon was
261 enigmatic due to the lack of any way of estimating the depth of incision of the tributary. This
262 uncertainty left room for numerous interpretations concerning the hypothetical digging of a
263 Messinian canyon by the Ardèche river. Some authors considered that the Ardèche had not incised
264 its valley or had only very slightly incised it during the Messinian (Sadier, 2013; Martini, 2019) while
265 others did not separate the river from its base level, which is the Rhône Messinian canyon (Baulig,
266 1953; Belleville, 1985; Mocochain *et al.*, 2006a,b, 2009; Tassy *et al.*, 2022).

267 ***2.3 Regional uplift since the Messinian***

268 It should be borne in mind that the current surface position of the markers derived from the
269 Messinian-salinity crisis is not that at their original altitudes. For example, the current transition from
270 marine to continental sedimentation in the Pliocene is observed at an altitude of ~ 130 m in several
271 places surrounding the Middle to Lower Rhône valley (Ballesio, 1972; Mocochain *et al.*, 2006a, b,
272 2009; Tassy *et al.*, 2022) and was confirmed by our own field study. According to eustatic sea-level
273 charts (Lisieki & Raymo, 2005; Miller *et al.*, 2020), this marker should be located between 0 and 40 m
274 above present sea level, indicating a regional uplift of around 90-130 m that occurred later than the
275 date of emplacement of this marker (estimated at ~ 4.7 Ma - Mocochain *et al.*, 2009) as already

276 proposed by Denizot (1952) and Mandier (1988). This uplift could be linked to the isostatic rebound
277 following glacial erosion of the Alps and/or the associated mantle upwelling, as well as to Pliocene
278 volcanism, as proposed by Olivetti et al. (2016) who suggest an uplift of around 200-300 m in the
279 French Massif Central. Gargani (2004b) estimated a post-Messinian uplift due to an isostatic rebound
280 of 20 to 170 m in the Tricastin area. Malcles et al. (2020) also suggest that part of this uplift in the
281 Cevennes area for the last 4 Ma, is due to isostatic readjustment caused by erosion.

282 **3 Dataset and methodology**

283 The dataset used for this study, which is composed of 11 seismic profiles, has been the property of
284 IRSN since 2020 (Fig. 3), it comprises nine multi-trace onshore profiles (P1, P2, P3, P4, P5, P6, P7, P9
285 and P10) acquired with vibroseis and geophones; plus two marine-type seismic profiles (P8C16 and
286 P8D16) acquired with an airgun system and a streamer on the Donzère-Mondragon channel.

287 Onshore profiles were recorded up to 3s in two-way travel time (TWT), the two channel seismic
288 profiles up to 2s TWT. A complementary seismic profile (94 MAR01) was also included in this study.

289 The complementary profile is one of the profiles acquired by ANDRA in the 1990s and reprocessed
290 more recently (Hollender *et al.*, 2015a; Hollender pers. Comm.). As we tried to unravel the recent
291 history of the Rhône valley, we focused on the upper part of the seismic profiles, up to 0.75s twt,
292 where the seismic signal is well recorded. We used the standard seismic-stratigraphic analysis
293 principles presented by Mitchum and Vail (1977) to characterise and define the seismic unit
294 architecture together with the geometry of their bounding surfaces (onlap, toplap, downlap and
295 truncations) and vertical stacking patterns. The seismic units defined on the seismic profiles were
296 then linked to previous studies and compared to those in a deep well at Codolet (BSS002CMTA)
297 located farther south (Ferry *et al.*, 1997) near the 94 MAR01 profile (Fig. 3). We performed the
298 seismic stratigraphic analysis on all the twt seismic profiles of the Tricastin area and afterwards
299 depth-migrated the various horizons based on the P-wave velocities retrieved from the depth-

300 converted P4 profile (see explanation below) which we considered to be representative of the local
301 geology of all seismic horizons that could exist in this area.

302 Depth conversion of seismic units requires the use of velocity data. Seismic reprocessing of seismic
303 profile P4, intersecting two canyons and featuring an intermediate island formed by Cretaceous-age
304 series, as demonstrated by the Grand-Malijac, Mirabelle and Pr  f  rence boreholes (see Fig. 4, 5), was
305 pivotal. We used an original methodology (following techniques used and described in Beccaletto *et al.*,
306 2011) aiming at specifying the shape of the Ard  che and Rh  ne paleo-canyons, the P-wave velocities of
307 the Messinian canyon filling units and the enclosing formations. This was achieved using a 2-step process
308 (velocity, deep static guiding) detailed in Supplementary material. As a result of this conversion, the
309 mean P-wave velocity of the Pliocene filling is ~2,200 m/s, in line with velocity of the Pliocene deposits
310 further south (Schlupp *et al.*, 2001), in the vicinity of Roquemaure-Pujaut.

311 **4 Results, interpretation and MES surface model**

312 **4.1 Well correlation**

313 A stratigraphic correlation of six selected boreholes, from Pierrelatte (BSS002BNBB) to Codolet
314 (BSS002CMTA), is given in Figure 4. The deepest well in the study area is the Mondragon well (drilled
315 to 1,838 m). It reached Hauterivian marls and crossed a major thrust below which more than 1000
316 m of Urgonian facies were revealed. The other wells drilled through sedimentary sequences ranging
317 from 70 m (Grand Malijac; BSS002BMYX) up to 834 m in thickness (Saint-Paul-Trois-Ch  teaux;
318 BSS002BNWH). Both the Pierrelatte and Saint-Paul-Trois-Ch  teaux wells reached the Urgonian
319 facies (Barremian in age), while those at Grand Malijac and Saint Paulet de Caisson (BSS002CLEB)
320 ended in the Cenomanian sandstones. Above the Cretaceous series, only Pliocene strata were
321 found, the base of which marked the Messinian Erosional Surface (MES). The thickness of the
322 Pliocene deposits varies considerably depending on whether the well is located close to or far from
323 a Messinian talweg axis. The Pierrelatte well revealed the occurrence of 269 m of Pliocene strata

324 comprised of 16 m of basal conglomerates followed by 100 m of continental fluvio-lacustrine
325 deposits, 130 m of azoic grey clays and marls and finally 23 m of marine bluish marls/clays (Ballesio,
326 1972). Until now, this was the deepest base of Pliocene known in the study area and was thought to
327 be relatively close to the Messinian talweg (Clauzon, 1982; Debelmas *et al.*, 2004). The Saint-Paul-
328 Trois-Châteaux well, drilled for hydrological purposes in 2003, revealed (from bottom to top): 264 m
329 of Barremian-Aptian limestones, 108 m of late Aptian (Gargasian) dark-grey marls and clays, 27 m of
330 azoic greyish sandy clays, 75 m of azoic grey clayey sands, 350 m of Pliocene dark-grey clayey marls
331 and finally 10 m of alluvium. According to the succession in this borehole, the base of the Pliocene is
332 at -302 m b.s.l., 89 m lower than in the Pierrelatte borehole. It also means the Saint-Paul-Trois-
333 Châteaux well is located closer to the talweg of the Messinian Rhône than the Pierrelatte well. The
334 102 m azoic interval made of sands and clays was not assigned to a specific interval (between 360 m
335 and 462 m in depth), because of the lack of biostratigraphic markers, hence it could belong to either
336 the Cretaceous series (Turonian sandstones) or the Pliocene. The interpretation of seismic profile
337 P8D16 will play a key role in overcoming this uncertainty.

338 Further southwest, the Grand Malijac well crossed a very thin (~3 m) Pliocene strata made of blue
339 marls, whose base is at an elevation of +30.7 m a.s.l. Although located close to Grand Malijac,
340 neither the Preference nor the Mirabelle (BSS002BNPG; Fig. 4) wells record any Pliocene. The area
341 surrounding the village of Lapalud suggests a paleo-interfluvial area. Further south, the Saint Paulet
342 de Caisson well, located on the present-day Ardèche river, revealed the occurrence of 142 m of
343 Pliocene grey marls with a few sandy intercalations. Here, the MES stands at -100m b.s.l. Ninety-
344 three metres of Pliocene marls were recorded in the Mondragon well, the basal 29 m being the
345 richest in sands and lenses of lignite. The Codolet well is located further south of the Mondragon
346 anticline, which crosses more than 443 m of Pliocene strata without reaching the MES. Four
347 Pliocene units, hereafter named PI1 to PI4 from bottom to top, were recorded in the Codolet well:
348 PI1 comprises 94 m of a sandy unit with some intercalations of lignite-bearing blue clays, PI2 is a
349 100-m thick unit richer in clay, PI3 follows with a 127-m thick unit mainly comprised of clays but still
350 fewer sandy beds, and finally the PI4 unit made of blue marls and clays (Ferry *et al.*, 1997). Based on

351 the succession of sedimentary facies described in Codolet, we tentatively propose a correlation of
352 P11 to P14 units in the Tricastin area.

353 **4.2 Seismic units**

354 Each seismic unit was first described using seismic profile P4, which is available in twt and depth
355 (Fig. 5) and then expanded to the other profiles and correlated with the well records. Seismic
356 interpretation was performed using IHS Kingdom suite seismic interpretation software. Seismic units
357 are grouped with respect to their acoustic signal (reflector amplitude and continuity).

358 *K1, K2 and K3 seismic units*

359 At the bottom of the P4 seismic profile is a seismic unit named K1, marked by rather transparent
360 facies, evolving towards the top to higher amplitude and more continuous reflectors, and is topped
361 by the most prominent feature made of three couplets of very high amplitude continuous reflectors.
362 The base of K1 unit was not interpreted in the seismic profiles. Aside from the base the K1 seismic
363 unit dips slightly eastwards in all the E-W seismic profiles, and is close to the surface at the western
364 end of profiles P1, P2 and P3 (Fig. 6). The depth converted model of profile P4 (Fig. 5) shows a deep
365 domain corresponding to the K1 seismic unit with fairly high velocities (between 3,500 m/s and
366 4,500 m/s, increasing downwards). This K1 seismic unit almost certainly corresponds to the Lower
367 Cretaceous level in Urgonian facies outcropping in Pierrelatte and close to the surface in profiles P6
368 and P7 (Fig. 7). In addition, along the P8D16 seismic profile, it was crossed by both the Pierrelatte
369 and Saint-Paul-Trois -Châteaux wells (Fig. 8, 10).

370 The K2 seismic unit, visible in the centre of the P4 seismic profile, is composed of lower amplitude
371 yet relatively continuous reflectors. The top of the K2 seismic unit is marked by a strong couplet of
372 reflectors. In more detail, the K2 seismic unit is made of two subunits of equal thickness in P4, the
373 lower one characterised by lower amplitude seismic facies. The K2 seismic unit tends to become
374 thinner towards the north of the study area, decreasing from ~200 ms in P4 to ~100 ms in profile P1

375 (Figs. 5 and 6) and thickens towards the south (profile P7; Fig. 7). Like the K1 unit, K2 dips eastwards.
376 The depth converted model of profile P4 shows mean interval velocities of 2,550 m/s in unit K2. This
377 interval, crossed by many wells (Fig. 4) is made of Aptian, Albian and Cenomanian marls, sandstones
378 and limestones. The low-amplitude reflectors observed on the lower part of unit K2 (Fig. 5, 6) could
379 correspond to grey Aptian marls (Gargasian level).

380 The overlying K3 unit is characterized by discontinuous, low- to moderate-amplitude reflectors,
381 although it displays occasional high-amplitude reflectors locally. The thickness of this unit varies
382 considerably as it is truncated by the Messinian erosion. For instance, the unit is missing in the
383 Pierrelatte, Saint-Paul-Trois-Châteaux and Saint-Paulet-de-Caisson wells (Fig. 4). K3 is missing in most
384 boreholes, except on (1) Grand Malijac where it corresponds to Turonian sandstone and (2) in the
385 Mondragon well, which exhibits a thick sequence made of Albian calcareous marls and coarse
386 sandstones evolving to sandy-clayey limestones of the Cenomanian. The K3 seismic unit is generally
387 better preserved from erosion toward the south of the study area (see profile P6 and P7, Fig. 7)
388 where its internal seismic facies feature high-amplitude reflectors toward the top. The depth
389 converted model of seismic profile P4 shows that the K3 unit is characterised by an interval velocity
390 of ~2,200 m/s.

391

392 *Messinian Erosional Surface (MES)*

393 In the Tricastin area, the MES most often cuts through K2 and K3 units, and reaches the K1 unit in
394 the southern part of the region (Fig. 5, 6, 8). Three main incisions were identified and correlated
395 across seismic profiles: the Rhône canyon (RC), the Ardèche canyon (AC) and a tributary of the
396 Ardèche (ATrC) (Figs. 5 to 9). Along the E-W seismic profiles, the main- and simultaneously the
397 deepest - incision is located at the eastern edge of the present-day Quaternary valley, west of the
398 Donzère-Mondragon channel. From the P2 seismic profile to the P4 seismic profile, the acoustic

399 depth of the deepest incision deepens southwards from ~500 ms to ~620 ms (Figs. 5, 6 and 9). This
400 incision is, without doubt, the Messinian Rhône canyon (RC in Figs. 5 to 9).

401 Unlike the other profiles, the P5 seismic line shows two adjacent canyons (Fig. 6): a western, narrow,
402 500-ms-deep canyon and a shallower one (300 ms deep). The most westerly canyon is also visible on
403 the southern part of the P7 seismic profile, at a depth of ~425 ms (Fig. 7). Being located at the
404 present-day exit of the Gorges of the Ardèche, this canyon is very probably the Messinian Ardèche
405 canyon (AC in Figures 6 and 7). The other shallower canyon can be interpreted as the course of a
406 tributary of the paleo-Ardèche river (ATrC in Figs. 5 and 6).

407 In seismic profile P7, the Ardèche tributary canyon appears as a shallow incision, north of the
408 Ardèche canyon (Fig. 7). A canyon is visible at a shallow level west of the P4 seismic profile, reaching
409 250 ms in depth (Fig. 5). This canyon may be the upstream part of the tributary canyon of the
410 Ardèche, with a N-S oriented course, east of the P7 seismic profile and the Lapalud area.

411 South of Mondragon, the 94MAR01 seismic profile, located alongside the Rhône, shows the
412 occurrence of a deep incision by the Messinian Cèze river (CC in Fig. 9), reaching a depth of ~530 ms.
413 Immediately to the south of the Cèze canyon, another incision reaching a depth of ~390 ms occurs
414 on the seismic profile, most probably corresponding to the Tave canyon (TC in Fig. 9) that today
415 joins the river Cèze just west of the seismic profile.

416

417 *Pliocene units (Pl-r, Pl1, Pl2, Pl3 and Pl4)*

418 Up to five successive seismic units of Pliocene age fill the canyon. They mostly onlap incisions, paleo-
419 topographies and anticlines (Fig 7, 8). Some of the Pliocene infill in the central part of canyons
420 displays a syncline-like geometry, that we interpret as the result of differential compaction.

421 On the eastern side of seismic profile P4 (Fig. 5), the basal unit is made of chaotic reflectors and presents
422 an irregular top, pinched towards the western border of the canyon. This unit is interpreted as a Mass-

423 Transport Deposit (MTD), and is referred to as Pl-r1 (r stands for reworked sediments and the 1 means
424 unit Pl1 onlaps onto it). This Pl-r1 unit is not a stratigraphic unit but rather a seismic facies unit. On profile
425 P4, it covers the western side of the Messinian canyon down to the centre, and also appears on seismic
426 profiles P4, P2, P9 and P10 (Fig. 5, 6 and 9) reaching up to 150 ms twt (~165 m with the overall Pliocene
427 filling velocity of 2,200 m/s) in seismic profile P2, south of Pierrelatte. The lateral extension of this unit
428 appears to be controlled by the paleo-topography of the Messinian incisions (Fig. 9). Interestingly, a
429 coeval basal Pl-r1 unit also appears on the flank of the Messinian canyon in both the Cèze canyon (Fig. 9)
430 and the Rhône canyon where it cuts through the Mesozoic carbonates. In the Tricastin area, this unit is
431 mostly onlapped by unit Pl1 and to a lesser extent by unit P2 (Fig. 9). Two other reworked series are
432 visible higher up in the Pliocene filling and are described hereafter with respect to the seismic unit
433 onlapping onto it.

434 The Pl1 unit onlaps the Pl-r1 unit and, overall, fills the base of the incisions. It mainly presents two seismic
435 facies: seismic facies 1 (SF1 in Fig. 10), made of relatively continuous and moderate to high amplitude
436 parallel reflectors, and seismic facies 2, made of moderate to low amplitude discontinuous reflectors
437 (SF2 in Fig. 10). It should be noted that seismic facies of Pl1 unit differs on seismic profiles shot in the
438 Donzère-Mondragon channel (see P8D16 seismic profile in Fig. 8) from those on the other seismic
439 profiles, probably due to the difference in acquisition techniques. The Pl1 unit was drilled in Saint-Paul-
440 Trois-Châteaux and Pierrelatte wells and is characterised by sands and clay/marls (Fig. 4). In Saint-Paul-
441 Trois-Châteaux, this interval, which is interpreted as Pl1 (Fig. 8) corresponds to the 102 m azoic interval
442 made of sands and clays which were not stratigraphically assigned by the drilling. Profile P8D16 clearly
443 shows that the upper high amplitude reflectors in the K2 seismic unit are eroded by the MES. The Pl1
444 unit is also the thickest unit filling the canyon, where its thickness reaches 300 m in the Rhône valley (Fig.
445 5) and approximately 330 m in the Ardèche canyon (Fig. 6, profile P5). Higher amplitude reflectors might
446 reflect sand bodies since in Saint-Paul-Trois-Châteaux, the Gamma-Ray (GR) log exhibits low values
447 typical of sandy intervals, like in Codolet well in the Cèze canyon (Fig. 10).

448 The PI2 unit which conformably overlies the PI1 unit, is relatively thin compared to PI1, with a thickness
449 ranging from ~80 to ~120 m, considering a mean velocity of 2,200 m/s. The PI2 unit is characterised by
450 two seismic facies: seismic facies 3, made of not wholly continuous parallel to divergent reflectors,
451 moderate in amplitude (SF3 in Fig. 10) and seismic facies 4, marked by moderate amplitude
452 discontinuous reflectors topped by higher amplitudes doublets (SF4 in Fig. 10). Pierrelatte and Saint-
453 Paul boreholes show that unit PI2 is more shaly and less sandy than unit PI1. In the Cèze canyon, unit
454 PI2 is marked by many lignite layers (Fig. 4). The mean thickness of the PI2 unit is relatively constant
455 throughout the Tricastin area (calculated as ranging from ~80 to ~120 m), although with slight thickening
456 southwards (profile P8D16, Fig. 8). The GR trend in Saint-Paul-Trois-Châteaux borehole shows a sharp
457 transition to higher values marking the occurrence of a clay-richer interval (Fig. 10). In Codolet, the GR
458 trend also shows higher values with spikes marking layers of blue clays and lignites (Fig. 10). A local MTD
459 occurs on the northern flank of the Ardèche canyon (light-grey PI-r2 unit on profile P5; Fig. 6). More
460 interestingly, the top of unit PI2 occurs at the steep shoulder of the Messinian canyon, where the canyon
461 widens significantly (Fig. 6, 7, 8, 9).

462 PI3 conformably overlies PI2, and onlaps onto the Messinian erosional surface. The contact between PI2
463 and PI3 is marked by a high amplitude couplet of reflectors, which are more visible on profiles P2, P4, P5
464 and P10. Thicker than unit PI2, unit PI3 is marked by three seismic facies: SF2 and SF3, as described for
465 units PI1 and PI2, plus seismic facies 5, which is made of moderate to high amplitude divergent reflectors
466 (SF5 in Fig. 10). Unit PI3 was crossed by many wells (Fig. 4) and reveals a composition of grey clays and
467 marls with local sand, silt or gravel layers. GR logs in both Codolet and Saint-Paul-Trois-Châteaux wells
468 also show higher values, in agreement with the shaly content of the PI3 unit (Fig. 9). On the western side
469 of seismic profile P4 (Fig. 5), a local MTD (PI-r3) is onlapped by unit PI3. In the Cèze canyon, this layer is
470 marked by the occurrence of thin layers of lignites. Even though unit PI3 mostly onlaps older structures
471 (Fig. 6, 7), in seismic profile P8D16 (Fig. 8), unit PI3 appears to be tilted onto the hanging wall of the
472 Mondragon frontal blind thrust (see fault F2 in Fig. 9 as well). A detailed view of this sector is provided in
473 Figure 11 and will be discussed later.

474 The shallow P14 unit is poorly imaged on the seismic reflection because processing did not focus on this
475 interval. One could however observe that this unit appears to be conformably deposited above unit P13
476 (Fig. 5). In terms of internal structures, unit P14 is marked by low amplitude and discontinuous,
477 sometimes transparent, reflectors, whereas in seismic profiles shot in the Donzere-Mondragon channel,
478 unit P14 is characterised by high amplitude reflectors (Fig. 8). When drilled, unit P14 is marked by the well-
479 known bluish clays and marls of the Pliocene, often found outcropping on the field (Ballesio, 1972). GR
480 trends in Saint-Paul-Trois-Châteaux and Codolet both show high values consistent with the clay-rich
481 filling (Fig. 10). It should be noted that the top of the seismic unit P4 is very difficult to interpret and that
482 contact with the Quaternary is not clear.

483

484 ***4.3 Construction of the MES surface model***

485 We used the Topo-to-Raster tool implemented in spatial analyst extension of Arcmap Desktop 10.6
486 version (ArcMap, ESRI) to construct a 3D morphology of the Messinian Erosional Surface. This
487 interpolation method makes it possible to create DEMs with consistent hydrological networks (e.g.
488 Hutchinson et al, 2011). The Topo-to-Raster tool interpolates elevations, and considers constraints
489 including isolines, measured elevations, and streams, for example. The output is a topography that is
490 consistent with drainage resulting from river erosion, which is the case for the Messinian Erosional
491 Surface.

492 In order to add constraints at depth, we carefully investigated the BRGM borehole subsurface
493 database (<https://infoterre.brgm.fr>) and selected all boreholes that either crossed the base of the
494 Pliocene or those that did not identify any Pliocene deposits but instead older strata below the
495 Quaternary. The altimetric base of the Pliocene was then extracted to create a table containing X, Y
496 and Z (Table S1 in supplementary material), which was then used to interpolate the MES in depth
497 using the Topo-to-Raster tool. To this end, a combination of (1) the depth-converted SEM seismic
498 horizon considering a constant VP velocity of 2,200 m/s as explained above, (2) the depth of the

499 Pliocene recorded in the boreholes located within the study area, (3) the altitude of the Pliocene
500 outcrop boundaries taken from geological maps (see dashed line in Fig. 2), (4) the path of the
501 Messinian talwegs deduced from our interpretation of reflection seismic data and hypothesised for
502 the area for which no data are available (area between Malataverne and the Donzère-Mondragon
503 Channel and the part of the Ardèche located north of Saint-Paulet-de-Caisson). (5) Some specific
504 altimetric points were added downstream (the Rhône canyon at a depth of around -800 m south of
505 Mondragon, Hollender pers. comm.; the Pujaut area where the canyon talweg is known to be at
506 ~ 900 m; Schlupp *et al.*, 2001, Hollender *et al.*, 2015b) in order to constrain the river flow in the GIS
507 tool. Figure 12 shows the resulting digital model together with the input data. The model is a
508 smoothed topography with a 50 m grid. The model is the result of combining the current
509 topography retained outside the limits of the Pliocene filling of the canyon and the topography
510 constructed from the various sources of information derived from our analysis as described
511 previously. This topography can be compared with the most recent proposed by Roure *et al.* (2009)
512 (see Figure S6 in Supplementary material for more information). From south to north, the following
513 topographic structures are observed: on the right bank, the Cèze canyon (imaged by ANDRA in the
514 1990s; Roux & Brulhet, 1997), on the left bank, the Aygues canyon (Bailly *et al.*, 2015).

515 In the Tricastin area, the model differs from that of Roure *et al.* (2009) in that the outlet of the
516 paleo-Ardèche is significantly offset to the south and connects to the paleo Rhône canyon south of
517 Lapalud island. This path is controlled by seismic profiles P7 and P5. The confluence zone is not
518 imaged, but its location to the south of the study area partly constrained by the narrowness of
519 Rhône canyon in the corridor between the Cretaceous shoulders of the Mondragon cluse and
520 seismic profile P8C16 that show no further incision toward the south.

521 East of Lapalud, the position of the Rhône canyon is constrained by outcrops of Pliocene marine
522 sands and marls in the city of Bollène. Further information was available thanks to the presence of a
523 few boreholes showing the hectometric thickness of the Pliocene. The canyon widens throughout
524 the area between Lapalud and Pierrelatte, and has an asymmetrical transversal profile (gentle

525 western edge and steep eastern edge). This widening seems to be associated with erosion facilitated
526 in this area by subcropping soft Aptian to Cenomanian formations. Further north, between
527 Pierrelatte and La Garde Adhémar, the canyon again becomes entrenched in the Cretaceous
528 limestone, which forms a cluse at this point. The Z-shaped talweg is constrained by its repeated
529 crossing of line P8D16. Further north, due to the absence of constraints, we chose to draw a straight
530 line towards Malataverne Pass. Finally, the Paleo-Rhone diverges from the present-day river that
531 flows in the “Donzère Défilé”; the canyon cut through the Malataverne Pass, as shown by detailed
532 geological outcrop and subcrop mapping (Camus, 2003). Further north, currently no data are
533 available to define the exact path, except those from scattered drill cores.

534 **5 Discussion**

535 ***5.1 Course, depth and morphology of the Messinian canyons***

536 Seismic line P3 is the only one that crosses the Messinian Rhône canyon close to perpendicular. Line
537 P3 shows an asymmetrical shape including: 1) a gently dipping western flank ($\sim 10^\circ$ or $\sim 18\%$, based
538 on the velocities used in the depth conversion of profile P4) that mostly follows Cretaceous
539 structural surfaces (even though slightly erosive), and 2) an eastern flank with an abrupt slope ($\sim 16^\circ$
540 or $\sim 29\%$). Thanks to the depth converted seismic profile P4, we were able to estimate the slope of
541 the canyon to be $\sim 14^\circ$ ($\sim 25\%$) from the shoulder of the canyon, down to its bottom (Fig. 5). This
542 asymmetry suggests that during Messinian period, the Rhône river progressively eroded the clastic
543 Cretaceous series until it reached the more resistant Urgonian, controlled by the east-dipping
544 structural slope.

545 The talweg of the Messinian canyon was not directly imaged north of Line P1. However, a past
546 drilling campaign revealed the presence of the Messinian canyon below the Malataverne area (Fig.
547 12; Camus, 2003). The ultimate depth of the Messinian talweg remains unknown, but interpolation
548 using data from the boreholes suggest a talweg at a depth of more than -220 m b.s.l. From that

549 point southwards, seismic reflection depth-conversion suggests a talweg at a depth of 460-470 m
550 b.s.l. at P2, -580/590 m b.s.l. at P3 and at least ~700 m at P4. The Messinian canyon is not
551 perpendicularly crossed by seismic profiles further south in the Tricastin area. Along the P5 seismic
552 profile, the Ardèche canyon reaches ~600 m b.s.l., meaning the Rhône canyon was even deeper
553 close to Mondragon. Depth estimates made it possible to compute an average slope of the
554 Messinian talweg of 2.8% (or 1.6°) between P2 and P5.

555 The Tricastin area is known to be the locus of an important increase in slope along the Rhône
556 canyon (Clauzon 1982; Beaudoin *et al.*, 1997) with an upslope profile estimated at between 0.1 and
557 0.2% (0.06 to 0.1°) compared to the downslope profile, which is estimated to be close to 1% (0.6°).
558 The assumption of a knickpoint in the talweg resulted from an incomplete set of depth control data:
559 the most important available data came from the Pierrelatte well crossing the base of the Pliocene
560 series at -235 m b.s.l. However, recent seismic reflection profiles show that the Pierrelatte well did
561 not reach the base of the canyon, which is much deeper, in the range of 460-470 m b.s.l. along P2.
562 Our results imply a deeper MES in the Tricastin area, and consequently, a less steep slope of the
563 talweg downstream of the study area. Considering a -700 m b.s.l. depth of the canyon at P4, -460-
564 470 m b.s.l. at P2, we estimated a slope of between 0.6% and 0.9% in the Tricastin area. Our
565 modelling of the MES gives an ~1% (0.6°) slope from Malataverne to the confluence of Ardèche and
566 Rhône rivers to the south. The results of this present study reveal a more regular Messinian profile
567 of the canyon, at least up to Malataverne in the north. Additional subsurface data north of
568 Malataverne would help identify the suspected knickpoint north of the study area.

569 Interestingly, on P1 and P2 (Fig.6), the MES displays a flat surface parallel to both the top of K2 and
570 the top of P12 seismic units, which are in lateral continuity across the shoulder of the Rhône and
571 Ardèche canyons. This flat surface seems to either follow the structural surface of K2 seismic unit in
572 seismic profile P1, or to erode through the K2 seismic unit in profile P2 (Fig. 6). To the south of the
573 Ardèche canyon, in seismic profile P7 (south of AC in Fig. 7), the topmost surface of P12 seismic unit
574 laterally corresponds to a flat surface following a structural surface on top of (or within) the K3

575 seismic unit. The shoulders of the Rhône and Ardèche canyons deepen toward the south: the
576 shoulder of the Rhône canyon being approximately -30 m b.s.l. on the P1 seismic profile (given the
577 velocities extracted from the depth converted seismic profile), -60 m b.s.l. along the P2 seismic profile
578 and the shoulder of the Ardèche canyon at approximately -100 m b.s.l. (Fig. 7). The flat surface
579 might have been generated during a base-level stagnation, during either the fall or the rise in sea
580 level.

581 In our study area, the PI2 seismic unit, the top of which is laterally continuous with the flat surface,
582 is made of sands and clays of continental origin (lignites in the Codolet well, Fig. 4). There is thus no
583 direct evidence of marine deposits at that depth that would favour a wave-cut surface during the
584 Pliocene reflooding like that seen offshore (Bache *et al.*, 2012). It is thus very likely that this flat
585 surface is the result of the development of an alluvial plain or a lake during a period of sea-level
586 stagnation.

587 Considering the abandonment surface of the Miocene located at +360 m a.s.l. in Saint-Restitut, the
588 difference in elevation between the flat surface and the previous abandonment surface of the
589 Miocene is at least 400 m considering the shoulder of the Rhône canyon along the P1 seismic
590 profile. This difference in altitude may increase to ~460 m, considering the Ardèche canyon shoulder
591 along P7 seismic profile. Could this flat surface have been generated during a sea-level drop of that
592 magnitude? The drop in sea level during the first stage of the MSC is estimated to range from 400 m
593 (Beaudoin *et al.*, 1997) to ~500 m (Gargani & Rigollet, 2007) in the Rhône canyon. The depth of the
594 flat surface fits within this range. This kind of flat surface has already been observed further south in
595 the Durance Messinian canyon (Clauzon *et al.*, 1995) and its genesis has also been linked to the first
596 stage of the MSC sea-level fall (Hippolyte *et al.*, 2020).

597 Is it possible that this surface was generated during the sea-level rise following the deposition of
598 evaporites in the central Mediterranean basin? The lateral continuity between the flat surface and
599 the PI2 unit argues in favour of a surface-forming process that would genetically link those features

600 during the Pliocene sea-level rise. Periods of stagnation in sea-level rise during the Pliocene
601 reflooding produced wave-cut surfaces in the Gulf of Lions and offshore Provence (Bache *et al.*,
602 2012, Tassy *et al.*, 2014), but none of those surfaces reach the altitude of the flat surface identified
603 underneath Tricastin. The Ardèche area was subject to the development of a subsurface karstic
604 network where the sea-level drop of the MSC was responsible for a deep flooded karst and a rise in
605 sea level produced *per ascensum* terracing of horizontal networks at +90 and +130 m a.s.l.
606 (Mocochain *et al.*, 2006a; Arfib & Mocochain, 2022). In addition, several wave-cut surfaces have
607 been identified 20 km south of Tricastin at +60 m and +100/105 m (Caziot, 1890). These
608 observations indicate oscillating reflooding during the Pliocene, however the limited lateral
609 extension of the above-mentioned sea-level stagnations suggest that none of those could have given
610 rise to such a large flat surface as that observed on the seismic profiles in the Tricastin area. The
611 development of such a wide flat surface at the top of the PI2 unit almost certainly marks a base-level
612 stagnation that lasted for a substantial period of time during the Pliocene reflooding. A forward
613 stratigraphic modelling approach including sea-level fluctuations and stagnations during the
614 reflooding would provide more insights into the creation of this surface.

615

616 **5.2 Interpretation of the canyon infill**

617 In the Western Mediterranean, most coastal rias Pliocene in age are filled with regressive deposits
618 marked by a Gilbert-type fan delta superimposed over debris flows (Clauzon *et al.*, 1995; Breda *et*
619 *al.*, 2007; Duvail, 2008). Such deposits are mostly found in areas located close to the apex of the
620 sedimentary system where transgressive deposits due to the reflooding of the Mediterranean Sea
621 are missing. In the Tricastin area, the successive PI1 to PI4 units, evolving from continental sands to
622 marine clays and shales, mark an overall transgression during the filling of the canyons, but no clear
623 deltaic systems such as Gilbert-type fan delta were observed in the seismic profiles. The stacking
624 pattern of the study area starting with sands evolving to marine clays is a pattern that has already
625 been identified in both the Pujaut graben (Ballesio, 1972) and the Cèze canyon (Ferry *et al.*, 1997).

626 Ferry et al. (1997) also concluded that within the Rhône canyon, the Pliocene denotes the complex
627 transgressive system tract of the Pliocene sea level rise, which apparently did not develop in the
628 coastal rias due to low sedimentation rate.

629 The significance of the various MTDs identified on the seismic profiles needs to be discussed. The
630 basal PI-r1 unit, observed on seismic profiles P2, P4, P9 and P10, is located on the western flank of
631 the Rhône canyon and seems to pinch out eastwards on profile P2 (Figs. 6 and 9). More importantly,
632 the basal PI-r1 unit pre-dates deposition of unit PI1 which onlaps over the MTD. On seismic profile
633 P9 and 91MAR01 (Fig. 9), the base of unit PI1 appears to be lower than the base of unit PI-r1,
634 suggesting an incision occurred between the deposition of unit PI-r1 and PI1. No wells have ever
635 been drilled in this unit, however some debris flows, sometimes called block formation (“Formations
636 à gros blocs” in the Languedoc area; Ambert, 1989), polygenic conglomerates or even olistoliths and
637 breccias, have been found unconformably over the Miocene and below the Pliocene shales,
638 covering the flank of the Cèze canyon (Ballesio and Truc, 1978), along the Rhône valley (Ballesio,
639 1972; Clauzon, 1978; Schlupp *et al.*, 2001) and even offshore (Bache *et al.*, 2012). Their origin along
640 the Rhône and the Cèze canyons is usually interpreted as the result of hillslope processes (scree
641 aprons). Ballesio and Truc (1978) also pointed to the close relationship between the occurrence of
642 these thick bodies and the vicinity of fractures and faults, which are assumed to have been active
643 during Alpine shortening. All these criteria lead us to assume PI-r1 deposits were emplaced during
644 the second stage of the MSC (5.6-5.46 Ma), i.e. during the massive drawdown in sea level. An
645 emblematic example of such deposits is the Carros Breccia, which is located on the western flank of
646 the Var Messinian canyon (Clauzon, 1978) between the MES and the marine Pliocene foresets. Map
647 and facies analyses clearly show that they are scree aprons deposited during the subaerial phase of
648 erosion at the base of an active relief in this case, a thrust front.

649 On seismic profile P5, the tributary of the Ardèche river (ATrC in Fig. 6) is partly filled by a MTD,
650 sandwiched between unit PI1 and the PI2 unit that onlaps onto it (light-grey polygon in Fig. 6). This
651 MTD dips toward the canyon axis, identifying its origin as the steep Turonian-Coniacian shoulder to

652 the north. The fact that this MTD is intercalated within the Pliocene filling suggests that slope
653 instabilities remained active at various places and times during the filling of the canyon caused by
654 reflooding. This continuing activity is also supported by the intercalation of another MTD between
655 the units PI2 and PI3 on seismic profile P4 (Fig. 5), most probably originating from the same
656 Turonian-Coniacian series of the Lapalud sector. The generation of MTDs triggered during sea-level
657 rise has not been recognised in seismic profiles either within the Cèze canyon or within the Pujaut
658 graben further south (Ferry *et al.*, 1997; Schlupp *et al.*, 2001). However, the breccias and olistoliths
659 pointed out by Ballesio (1972) at the surface along the Cèze canyon may be the best analogues of
660 those higher MTDs. Similar boulders are recorded in Roussillon at the boundary of the granitic
661 basement along the Têt river canyon (Clauzon *et al.*, 2015a): in this case, they are imbricated with
662 marine foresets but against the erosional surface. As a result, it is hard to decipher if they are coeval
663 to the sub-aerial period or if the slope continued to be eroded after the submersion.

664

665 **5.3 Identification of structures and deformations**

666 Identification of faults and of their apparent vertical displacement depends on the seismic
667 resolution (dominant frequency spectrum of our dataset between 50 and 100 Hz) as well as on
668 processing issues (see methods section). It is therefore difficult, if not impossible, to detect faults
669 with a vertical offset of less than 50 m in the Urgonian and 4 to 10 m in the most superficial levels.
670 However, experience shows that ruptures usually occur on pre-existing structures (as was the case
671 on the La Rouvière fault during the Le Teil earthquake, see Ritz *et al.*, 2020). Consequently, it is
672 important to identify deep seated faults to identify potential fault rupture for seismic hazard
673 assessment.

674 In addition, the identification of "structures" on seismic profiles should be interpreted with caution
675 as most seismic profiles have not benefitted from static correction, particularly in our case where
676 there is a significant "pull down" effect of reflected waves due to the presence of the Plio-

677 Quaternary filling of the canyon, which may produce fault-like or fold-like structures (see example in
678 Hanot and Thiry, 1999; Beccaletto et al., 2011). However, the structures described below display
679 offsets that are large enough to be considered as faults or folds.

680 **5.3.1 Faults and folds affecting the Cretaceous series**

681 N-S oriented profiles P8D16, P6 and P7 cross a broad ENE-WSW oriented anticline affecting the
682 Cretaceous series (Urgonian and locally Aptian). The maximum amplitude of this anticline is around
683 500 m computed with 2,200 m/s for post-Urgonian sequences, for a distance of around 7 km. This
684 structure correlates with the Echavarellas anticline (Fig. 13) and also accounts for the small outcrop
685 of Urgonian limestone in Pierrelatte due to additional normal faulting of the anticline axial plane.
686 This large structure is affected by shorter wavelength series of folds, ENE-WSW oriented (Fig. 13),
687 which can be identified on profiles P6 and P7 (Fig. 7). These N80-trending structures run parallel to
688 the Mondragon fold in the Uchaux massif, which was created during the Pyrenean shortening
689 (between the Palaeocene and Oligocene; see Ballas *et al.*, 2014 and references therein). At La
690 Garde-Adhémar, the Echavarellas anticline is unconformably covered by Oligocene marls that
691 overlie Aptian (Gargasian) marls to the south and Albian glauconitic sands to the north.

692 The Echavarellas anticline hinge is affected by a large fault (hereafter PF for Pierrelatte Fault, Fig. 13)
693 which offsets the Urgonian top by around 0.2s twt (500 m considering a VP velocity of 4,500 m/s in
694 the Urgonian) on profile P7. This offset reaches at least 0.1 s on profile P6 and is clearly visible on
695 profile P8D16 even though its offset remains difficult to compel (Fig. 7 and 8). We also identified the
696 Pierrelatte fault at the western end of the P2 profile (Fig. 6), but again the offset of this fault cannot
697 be estimated due to the fault orientation running oblique to the seismic profile. The Pierrelatte fault
698 shows a normal component, it offsets the Urgonian limestones and the overlying Aptian and is
699 truncated by the MES. The age of this fault is post Aptian and predates the formation of the MES.
700 Ballas *et al.* (2014), described normal faults of nearly the same strike in the Uchaux massif, 12 km to
701 the south (Mondragon, Mornas fault) and attributed their activity to the Oligo-Early Miocene

702 extension. The fault could therefore have been active during this geodynamic episode. However, the
703 position of this Pierrelatte fault in the extrados of this regional-scale anticline could also be
704 explained mechanically by the local extension of the anticline's hinge during the Pyrenean tectonic
705 episode. This fault has no clearly identified extension to the east (a few faults of similar direction are
706 mapped to the north of Clansayes) and is not mapped on the eastern limb of the Saint Remèze
707 dome to the south of Bourg Saint Andéol, where one would expect to find it. Apart from this major
708 fault identified on 3 profiles, minor structures have been interpreted cutting the Cretaceous series,
709 and do not appear affect the overlying Pliocene fill.

710 To the south of the Tricastin area, on profile P8C16, the deformation is clearly more pronounced.,
711 Combes & Carbon (1997) and Ballas *et al.* (2014) have shown that the Mondragon-Uchaux anticline
712 is a fault-propagation fold Pyrenean in age, later intersected by ~E-W normal faults. The Pyrenean
713 shortening is marked in profile P8C16 by the occurrence of south-dipping blind thrusts noted F1 and
714 F2 (Fig. 8, 13), F2 being the northern front thrust accommodating the Mondragon fault propagation
715 fold. Projection of the Mondragon borehole shows fault F2 is responsible of the duplication
716 identified in the Mondragon borehole (two occurrences of the Aptian/Urgonian succession:
717 BSS002CLTG). The F1 fault located further south, is most probably a splay of the Mondragon thrust,
718 as proposed by Combes & Carbon (1997). P8C16 displays a 0.2s twt offset of K3 series, some 2 km
719 north of F2. Although the seismic image does not clearly show the nature of this offset, the
720 Oligocene Dessoulière Fault that strikes N80°E (Combes & Carbon, 1997) may correlate with this
721 structure, noted F3 (Fig13).

722 **5.3.2 Deformation of the Plio-Quaternary canyon filling**

723 Seismic profiles reveal no folding or reflector offset at the scale of the seismic reflection resolution.
724 However, most profiles display thickening of the Pliocene sequence toward the canyon axis. While a
725 "pull-down" effect is likely (thicker series are slower and therefore appear even thicker on double-
726 time sections), the amplitude of this syncline geometry is nonetheless significant. It can also be seen

727 on profile P4, which has benefitted from static corrections (cf. Fig 5, profile P4 corrected for depth).
728 We suggest that this long-wavelength deformation may be linked to the differential compaction of
729 sediments along the canyon edges as it has been demonstrated and modelled close to escarpment
730 (Carminati & Santantonio, 2005). Such pattern has also been identified in the Cèze canyon (Ferry *et*
731 *al.*, 1997).

732 Finally, above the Mondragon fault propagation fold, on profile P8C16, we observed a south-dipping
733 bedding in the Pliocene fill (unit PI3) on the hanging wall (black arrows in Fig. 11, with apparent dip
734 reaching $\sim 15^\circ$) and north dipping bending reflector over the emergence or the Mondragon thrust
735 (white arrows in Fig. 11, with apparent dip reaching $\sim 30^\circ$). In our interpretation, these layers appear
736 to be truncated by the upper level PI4. This suggests a Pliocene reactivation of the Mondragon
737 thrust, during PI3 and prior to PI4 deposition. This north-south component shortening would be
738 coherent with compressive Quaternary activity observed in Courthézon near the Nîmes Fault and on
739 the La Rouvière Fault on the Cévennes Fault system (Bellier *et al.*, 2021; Ritz *et al.*, 2021). These
740 observations suggest that further investigation is needed to evaluate the recent (e.g. Plio-
741 Quaternary) tectonics in this area.

742 If the observed clinofolds originate from a sedimentary process (black and white arrows in Fig. 11),
743 they could represent steeply dipping clinofolds such as foreset beds of a Gilbert-type fan delta,
744 widely recognised along the Mediterranean coasts during the reflooding of the Mediterranean Sea.
745 However, if this is the case, such a thick delta would require an important lateral feeder system,
746 most probably from a tributary of the Rhône river, which is enigmatic.

747 **5.4 The Ardèche: from the canyon to the karst**

748 The present-day Ardèche canyon is incised into the Urgonian facies limestone and displays an
749 average slope of 1%. Marine Pliocene sediment found in the lower part of the present-day gorges
750 indicates that the current river course is inherited from the Messinian evolution (Ballesio, 1972;
751 Pascal *et al.*, 1989; Mocochain *et al.*, 2006b).

752 Downstream of the gorges, the seismic profiles interpreted in this contribution clearly show the
753 excavation of a deep and narrow canyon, visible on profile P7 at a depth of around 460 m b.s.l. (425
754 ms twt, Fig. 7) and on profile P5 at a depth of around 600 m b.s.l. (500 ms twt, Fig. 6). The canyon
755 cuts through the post-Urgonian Cretaceous formations that are richer in clastics and easier to erode
756 than the Urgonian bio-constructed limestone. This suggests the incision was halted by the Urgonian
757 limestone. The canyon axis interpreted on the P7 and P5 profile, which are 2,300 m apart, indicates
758 a longitudinal slope of approximately 6% towards the SE, which is equal to the regional dip of the
759 Urgonian limestone.

760 The Messinian Ardèche longitudinal profile therefore displays a significant increase in slope in the
761 area of the present-day outlet of the gorges. Incision into the silico-clastic dominated K3 and K2
762 sequences reached the Urgonian limestone immediately downstream of this point (see P5 on Fig. 6).
763 This resulted in a hydrogeological window that allowed the river water flux to take a shortcut
764 through the deep karstic network incised into the Urgonian limestone, to connect with the base
765 level represented by the Rhône canyon. As soon as these karstic networks developed beneath the
766 gorges, the erosion within the canyon downstream may have slowed down considerably. This
767 decrease in subaerial erosion would explain why the Ardèche canyon did not cut deeper into the
768 Urgonian limestone massif.

769 The deep karstic system ceased its activity during reflooding of the Mediterranean. The deep karst
770 was then buried under Pliocene sediments, leaving only the upstream parts of the submerged
771 networks, which currently form a set of Vaclousian systems (Arfib and Mocochain, 2022; Mocochain
772 et al., 2006a; 2011).

773 **6 Conclusions**

774 Our study showed that the Rhône canyon in the Tricastin area is up to several hundred metres
775 deeper than previously estimated (Clauzon, 1982; Roure et al., 2009). Depth converted seismic

776 profiles gave us access to seismic velocities of the canyon infill and allowed us to estimate the depth
777 of the Rhône canyon to range from -400 to -700 m b.s.l. in the area. In addition, a deep and narrow
778 canyon was imaged in the area of the lower reaches of present-day Ardèche river, which we interpret
779 as the Messinian Ardèche canyon. This canyon most probably merges with the Messinian Rhône
780 canyon south of Mondragon. Prior to this study, this deep Ardèche canyon has never been imaged
781 (see Roure et al., 2009 map in Supplement material). The Rhône and Ardèche canyon morphologies
782 widen at various locations following a flat surface located between -60 to -100 m b.s.l. We interpret
783 this relatively flat surface to be the result of a sea-level stagnation during the Pliocene reflooding.

784 The infill of the Rhône canyon started with the occurrence of a large basal MTD, located below the
785 Tricastin nuclear site, certainly deposited during the sea-level fall of the Mediterranean Sea after 5.6
786 Ma as it is overlapped by stratified Pliocene continental deposits. The overlying Pliocene infill of the
787 Rhône and Ardèche canyons consists of four seismic units that represent an overall transgressive
788 trend related to the reflooding of the Mediterranean Sea at the end of the MSC. At least two other
789 generations of MTDs took place during the rise in the level of the Mediterranean Sea. Their proximity
790 to interfluvial hills made of Cretaceous clastics certainly explains their genesis. No regressive system
791 tract was found underneath Tricastin, meaning it has been eroded above the present-day Rhône
792 alluvial plain.

793 From a structural point of view, the northern part of the Tricastin area is marked by ENE-WSW folds
794 affecting the Cretaceous, parallel to structures in the Uchaux massif. The seismic reflection data
795 indicate that the main structure is the continuation of the Echavarellas anticline which is faulted in its
796 extrados (Pyrenean faulting?) in the same direction, marking the Pierrelatte fault. The Uchaux
797 structures can be extrapolated downwards, where they show south-dipping thrusts marking the fault
798 propagation fold of the Uchaux massif. Pliocene reflectors appear to be deformed above the hinge
799 zone of the Mondragon anticline, reflecting possible recent reactivation of that structure. The latter
800 is of importance for future research on recent activity of tectonic structures as the area is subject to
801 low to moderate seismicity.

802 In a broader perspective, ongoing research dealing with seismic hazard and seismic wave
803 amplification below nuclear sites will greatly benefit from this study as we have contributed a
804 considerably more detailed subsurface geological model.

805 **Acknowledgments**

806 This work received support from the French government under the France 2030 investment plan, as
807 part of the Initiative d'Excellence d'Aix-Marseille Université - A*MIDEX (AMX-19-IET-012) and from
808 the Research Federation ECCOREV (FR 3098; Aix-Marseille Univ., CNRS, INRAE, IRSN, CEA, Univ.
809 Toulon, Univ. Avignon, Univ. Nîmes). Interpretation of seismic profiles benefited from academic
810 licence of S&P Kingdom software provided to IStep (Sorbonne Université). Ludovic Peignard is also
811 warmly thanked for providing a research licence of the EarthQuick software.

812 The authors thank Francois Lavoué for fruitful discussions on the canyon geometry and model
813 implementation for the numerical simulation of site effects. Sincere thanks are also due to Hervé
814 Jomard and Stéphane Baize for discussion and field participation on the Pliocene paleo-beaches and
815 paleo-notches. Vincent Ollivier, Nicolas Cathelin, Jean-Claude Hippolyte, Jules Fleury, Estelle Hanouz,
816 Jean-Pierre Suc and Gilles Dromart are thanked for fruitful discussions during a workshop organized
817 in November 2021 and various fieldtrips. Fabrice Hollender from CEA is warmly thanked for providing
818 reprocessed data on the seismic profile 94MAR01.

819 Sylvain Pouliquen and Christophe Vergniaux from EDF for discussion and data exchanges on the
820 seismic processing with CDP company, Didrik Vandeputte and the city hall of Saint-Paul-Trois-
821 Châteaux who provide us the eponymous borehole documents.

822 Seismic data use and publication was granted by ENGIE company to IRSN in the framework a non-
823 exclusive licence contracted in June 2020. We thank Hubert Mignot who made these data available.
824 We would also like to pay tribute to our colleague Christophe Clément, who helped us obtain the
825 ENGIE profiles and supported us at the beginning of this project.

826 Michel Séranne and Ferran Estrada are warmly thanked for their constructive reviews that helped
827 improving significantly the manuscript.

828 **References**

- 829 Ambert, P. 1989. Les formations à blocs messiniennes du piémont du Languedoc Central:
830 implications tectoniques et corrélations régionales. *Comptes rendus de l'Académie des sciences.*
831 Série 2, Mécanique, Physique, Chimie, Sciences de l'univers, Sciences de la Terre, 309(20), 2077-
832 2084.
- 833 Arfib, B., Mocochain, L. 2022. Deep flooded karsts of south-eastern France—Genesis and
834 hydrodynamic functioning. *Karstologia*, 79, 39-44.
- 835 Arthaud, F., Laurent, P. 1995. Contraintes, déformation et déplacement dans l'avant-pays Nord-
836 pyrénéen du Languedoc méditerranéen. *Geodinamica acta*, 8(3), 142-157.
- 837 Arthaud, F., & Matte, P. 1975. Les décrochements tardi-hercyniens du sud-ouest de l'Europe.
838 Géométrie et essai de reconstitution des conditions de la déformation. *Tectonophysics*, 25(1-2), 139-
839 171.
- 840 Bache, F., Olivet, J. L., Gorini, C. et al. 2009. Messinian erosional and salinity crises: View from the
841 Provence Basin (Gulf of Lions, Western Mediterranean). *Earth and Planetary Science Letters*, 286(1),
842 139-157. <https://doi.org/https://doi.org/10.1016/j.epsl.2009.06.021>.
- 843 Bache, F., Popescu, S.-M., Rabineau et al. 2012. A two-step process for the reflooding of the
844 Mediterranean after the Messinian Salinity Crisis. *Basin Research*, 24(2), 125-153.
- 845 Bailly T., Combes P., Dunand F. et al. 2015. Inter-comparaison des méthodes H/V et sismique
846 réflexion pour l'imagerie des canyons messiniens). 9ème Colloque National AFPS 2015.
- 847 Baize, S., Cushing, M., Lemeille, F., Granier, T., Grellet, B., & Carbon, D., 2002. Inventaire des indices
848 de rupture affectant le quaternaire, en relation avec les grandes structures connues, en France

849 métropolitaine et dans les régions limitrophes. *Mémoires de la Société géologique de France*
850 (1924), 175, 1-141.

851 Ballas, G., Soliva, R., Benedicto, A., Sizun, J.-P. 2014. Control of tectonic setting and large-scale faults
852 on the basin-scale distribution of deformation bands in porous sandstone (Provence, France). *Marine*
853 *and Petroleum Geology*, 55, 142-159. doi:<https://doi.org/10.1016/j.marpetgeo.2013.12.020>

854 Ballesio, R. 1972. Étude stratigraphique du Pliocène rhodanien (PhD). Docum. Lab. Géol. Fac. Sci.
855 Lyon, n° 53, 333 p.

856 Ballesio, R., Truc, G. 1978. L'Infra-Pliocène : nouveaux témoins dans le bassin du Rhône : les brèches à
857 éléments oligocènes de la vallée de la Cèze. Documents des Laboratoires de Géologie de la Faculté
858 des Sciences de Lyon, 72, 71-77.

859 Baulig, H. 1953. Les hauts niveaux de base du Pliocène. *Géocarrefour*, 28(3), 205-221.

860 Beaudoin, B., Accarie, H., Berger, et al., 1997. Caractérisation de la crise messinienne et de la
861 réinondation pliocène. *Compte-Rendu des Journées Scientifiques ANDRA, Bagnols-sur-Cèze*, 20-21.

862 Beccaletto, L., Hanot, F., Serrano, O., Marc, S., 2011. Overview of the subsurface structural pattern of
863 the Paris Basin (France): Insights from the reprocessing and interpretation of regional seismic lines.
864 *Marine and Petroleum Geology*, 28, 4, 861-879.

865 Belleville, L. 1985. Hydrologie karstique: géométrie, fonctionnement et karstogenèse des systèmes
866 karstiques des gorges de l'Ardèche. Ph. D. Thesis, Univ. Sc. Med, Grenoble, France, 228 pp.

867 Bellier, O., Vergely, P. 1987. Etats de contraintes et tectogenèse cénozoïque du plateau calcaire de
868 basse Ardèche (France). *Comptes rendus de l'Académie des sciences. Série 2, Mécanique, Physique,*
869 *Chimie, Sciences de l'univers, Sciences de la Terre*, 305(17), 1379-1382.

870 Bellier, O., Cushing, E. M., Sébrier, M. 2021. Thirty years of paleoseismic research in metropolitan
871 France. *Comptes Rendus. Géoscience*, 353(S1), 339-380.

872 Besson, D. , 2005. Architecture du bassin rhodano-provençal miocène (Alpes, SE France): Relations
873 entre déformation, physiographie et sédimentation dans un bassin molassique d'avant-pays. Ph. D.
874 Thesis , École Nationale Supérieure des Mines de Paris, France, 438 pp.

875 Bollinger, L., Le Dortz, K., Duverger, C., Vallage, A., Marin, S., Leroy, Y. M. 2021. Seismic swarms in
876 Tricastin, lower Rhône Valley (France): review of historical and instrumental seismicity and models.
877 *Comptes Rendus. Géoscience*, 353(S1), 585-606.

878 Bonijoly, D., Perrin, J., Roure, F., et al., 1996. The Ardèche palaeomargin of the South-East Basin of
879 France: Mesozoic evolution of a part of the Tethyan continental margin (Géologie Profonde de la
880 France programme). *Marine and Petroleum Geology*, 13, 607–23.

881 Breda, A., Mellere, D., Massari, F. 2007. Facies and processes in a Gilbert-delta-filled incised valley
882 (Pliocene of Ventimiglia, NW Italy). *Sedimentary geology*, 200(1-2), 31-55.

883 Camus, H. 2003. Vallées et réseaux karstiques de la bordure carbonatée sud cévenole: Relations
884 avec la surrection, le volcanisme et les paléoclimats. PhD, Bordeaux 3, 438 p.

885 Carminati, E., Santantonio, M. 2005. Control of differential compaction on the geometry of
886 sediments onlapping paleoescarpments: Insights from field geology (Central Apennines, Italy) and
887 numerical modeling. *Geology*, 33(5), 353-356.

888 Caziot M., 1890. Étude sur le bassin pliocène de Théziers-Roquemaure (Gard). *Bull. Soc. Géol. France*,
889 vol. 19, 205-219.

890 CIESM (Antón, J., Çağatay, M.N., de Lange, G. et al. 2008. Executive summary. In: The Messinian
891 Salinity Crisis From Mega-Deposits to Microbiology – A Consensus Report (Ed. by F.Briand) CIESM
892 Workshop Monographs, 33, 7–28.

893 Champenois. M., Conquy Y., Desoignies J., Henry J. 1971. Carte géol. France (1/50 000), feuille
894 Orange (914). Orléans : BRGM. Notice explicative par Champenois, M., Conquy, Y., Desoignies, J.
895 (1971), 13 p.

896 Champion, C., Choukroune, P., Clauzon, G. 2000. La déformation post-Miocène en Provence
897 occidentale. *Geodinamica Acta*, 13(2-3), 67-85.

898 Clauzon, G. 1974. L'hypothèse eustatique et le creusement prépliocène de la vallée du Rhône. In:
899 *Annales de Géographie*, t. 83, n°456, pp. 129-140; <https://doi.org/10.3406/geo.1974.18930>

900 Clauzon, G. 1978. The Messinian Var canyon (Provence, Southern France)—paleogeographic
901 implications. *Marine Geology*, 27(3-4), 231-246.

902 Clauzon, G. 1982. Le canyon messinien du Rhône: une preuve décisive du “Desiccated deep-basin
903 model ” (Hsu, Cita, Ryan, 1973). *Bull. Soc. Géol. France*, 24, 597–610.

904 Clauzon G., Aguilar JP., Delannoy JJ. et al., 1992. Genèse et évolution du piémont néogène subalpin
905 du Bas Dauphiné, Travaux URA 903, CNRS, 19, 78p.

906 Clauzon G., Rubino J.L. Savoye B. 1995. Marine Pliocene Gilbert-type fan deltas along the French
907 Mediterranean coast. A typical infill feature of preexisting subaerial Messinian canyons – 5ème
908 Congrès Français de Sédimentologie, Field Trip Book, Publ. ASF, Paris, n° 23, p. 145-222.

909 Clauzon, G., Suc, J. P., Gautier, F., Berger, A., Loutre, M. F., 1996. Alternate interpretation of the
910 Messinian salinity crisis: controversy resolved?. *Geology*, 24(4), 363-366.

911 Clauzon, G., Fleury, T.-J., Bellier, O., Molliex, S., Mocochain, L., Aguilar, J.-P. 2011. Morphostructural
912 evolution of the Luberon since the Miocene (SE France). *Bull. Soc. Géol. France*, 182 (2), pp. 95-110.
913 DOI: 10.2113/gssgfbull.182.2.95

914 Clauzon, G., Le Strat, P., Duvail C. et al. 2015a. The Roussillon Basin (S. France): A case-study to
915 distinguish local and regional events between 6 and 3 Ma. *Marine and Petroleum Geology*, 66, 18-40.

916 Clauzon, G., Suc, J.-P., Do Couto, D. et al. 2015b. New insights on the Sorbas Basin (SE Spain): The
917 onshore reference of the Messinian Salinity Crisis. *Marine and Petroleum Geology*, 66, 71-100.
918 <https://doi.org/https://doi.org/10.1016/j.marpetgeo.2015.02.016>

- 919 Combes P., Carbon D. 1997. Géologie structurale du Gard rhodanien entre les failles de Nîmes et des
920 Cévennes. Poster GG13. Atlas des Posters Bagnols-sur-Cèze, 26-27.
- 921 Debelmas J., Ballesio R., Brochier J.L., Fourneaux C., Moûtier L., Triat J.M. 2004. Carte géol. France
922 (1/50 000), feuille Valréas 2e édition (890). Orléans : BRGM. Notice explicative par J. Debelmas, avec
923 la collaboration de R. Ballesio, J.L. Brochier, C. Fourneaux, L. Moûtier, J.M. Triat (2004), 75 p.
- 924 Demarcq, G. 1960. Observations à propos de la série pliocène du sondage de Pierrelatte (Drôme).
925 *C.R. Acad. Sci., Paris*, 250, 4013-4015.
- 926 Demarcq, G., 1970. Étude stratigraphique du Miocène rhodanien, Mémoires du B.R.G.M. 61.
927 B.R.G.M., Paris.
- 928 Denizot, G., 1952. Le Pliocène dans la vallée du Rhône. *Géocarrefour*, 27(4), 327-357.
- 929 Dix, C. H., 1955. Seismic velocities from surface measurements. *Geophysics*, 20(1), 68-86.
- 930 Duvail, C. 2008. Expression des facteurs régionaux et locaux dans l'enregistrement sédimentaire
931 d'une marge passive. Exemple de la marge du Golfe du Lion, étudiée selon un continuum terre-mer
932 (PhD), Université de Montpellier 2, 265 p.
- 933 Ferry, S., Rubino, J.L., 1989. Mesozoic eustacy record on western Tethyan margins. Guide-book : post-
934 meeting field trip in the vocontian trough (25th-28th November 1989), 2ème Congrès français de
935 sédimentologie, Lyon, 23rd-24th November 1989, Paris; Association des sédimentologues français.
- 936 Ferry S., Ballesio R., Monier P. 1997. Modalités du remplissage sédimentaire de la ria pliocène du
937 Rhône. Problèmes en suspens après les premiers travaux ANDRA. Poster GG11. Atlas des Posters
938 Bagnols-sur-Cèze, 22-23.
- 939 Fontannes, F. 1882. Notes sur l'extension de la faune pliocène dans le Sud-Est de la France. *Bull. Soc.*
940 *Géol. France*, 3(2), 103-141.

941 Froment, B., Cushing, E. M., Gélis et al. 2022. First 3D characterization of the Rhône Messinian
942 Canyon in the Tricastin area from complementary geophysical approaches. In 3rd European
943 Conference on Earthquake Engineering & Seismology, Bucharest (Romania).

944 Gargani, J., 2004a. Eustatisme, érosion et isostasie flexurale: modélisation numérique appliquée au
945 Rhône messinien. *Comptes Rendus Géoscience*, 336(10), 901-907.

946 Gargani, J. 2004b. Modelling of the erosion in the Rhône Valley during the Messinian crisis (France).
947 *Quat. Int.*, 121, 13–22.

948 Gargani, J., Rigollet, C. 2007. Mediterranean Sea level variations during the Messinian salinity crisis.
949 *Geophysical Research Letters*, 34(10). <https://doi.org/https://doi.org/10.1029/2007GL029885>

950 Gélis, C., Cauchie, L., Cushing, E. M. et al. 2022. Estimation of the local seismic amplification on an
951 industrialized site in the French Rhône valley. *Pure and Applied Geophysics*, 179(6):2119-2145,
952 doi:10.1007/s00024-022-03069-x.

953 Guennoc, P., Gorini, C., Mauffret, A. 2000. Histoire géologique du Golfe du Lion et cartographie du
954 rift oligo-aquitainien et de la surface messinienne. *Géologie de la France*, (3), 67-97.

955 Guérin, R. 1973. Un exemple du rôle de la tectonique et de la microtectonique dans la géométrie des
956 écoulements karstiques fossiles et actuels : le Bas-Vivarais calcaire. Ph. D. Thesis, Montpellier Univ.,
957 France. 113 pp.

958 Hanot, F., Thiry, M. 1999. Anomalies sismiques dans la craie et déformations superposées dans les
959 formations tertiaires du sud-est du bassin de Paris. *Bull. Soc. Géol. France*, 170(6), 915–926.

960 Hippolyte, J. C., Suc, J. P., Gorini, C., Rubino, J. L., Do Couto, D. 2020. La Méditerranée s’assèche à la
961 fin du Messinien. In BRGM Editions (Ed.), *La géologie des Bouches du Rhône : roches et paysages*
962 remarquables, 145-160.

963 Hollender, F., Cushing, E.M., Dussouillez, P. et al. 2015a. Evaluation of site effect features of Miocene
964 paleo-canyons in south eastern France using ambient vibration methods, Presented at the
965 Conference: SSA 2015 Annual Meeting, 21-23 April Pasadena, USA.

966 Hollender, F., Cushing, E.M., Gelis, C. et al. 2015b. Contribution of ambient vibration measurement
967 methods for characterization of paleo-Messinian canyons in the southeastern France. 9ème Colloque
968 National AFPS 2015.

969 Hsü, K., Ryan, W., Cita, M., 1973. Late Miocene Desiccation of the Mediterranean. *Nature* 242, 240–
970 244. <https://doi.org/10.1038/242240a0>

971 Hutchinson, M.F., Xu, T. Stein, J.A. 2011. Recent Progress in the ANUDEM Elevation Gridding
972 Procedure. *Geomorphometry*, 2011, 19-22.

973 Jomard, H., Cushing, E. M., Palumbo, L., Baize, S., David, C., and Chartier, T. 2017. Transposing an
974 active fault database into a seismic hazard fault model for nuclear facilities—Part 1: Building a
975 database of potentially active faults (B DFA) for metropolitan France. *Nat. Hazards Earth Syst. Sci.*, 17,
976 1573–1584.

977 Lacombe, O., Jolivet, L. 2005. Structural and kinematic relationships between Corsica and the
978 Pyrenees-Provence domain at the time of the Pyrenean orogeny. *Tectonics*, 24(1), TC1003.

979 Lesueur, J.L., Rubino, J.L., Giraudmaillet, M., 1990. Organisation et structure internes des dépôts
980 tidaux du Miocène rhodanien. *Bull. Soc. géol. Fr., Paris, sér. 8, t. 6, n° 1*, pp. 49-65.

981 Lisiecki, L.E., Raymo, M.E. 2005. A Pliocene–Pleistocene stack of 57 globally distributed benthic δ¹⁸O
982 records. *Paleoceanography*, 20, 1.

983 Malartre, F., 1994. Stratigraphie séquentielle du Crétacé supérieur du bassin vocontien occidental
984 (Sud-Est, France). Comparaison avec d’autres bassins. *Docum. Lab. Géol. Lyon*, 131, 213.

985 Malcles, O., Vernant, P., Chéry, J., et al., 2020. Determining the Plio-Quaternary uplift of the southern
986 French Massif-Central; a new insight for intraplate orogen dynamics. *Solid Earth*, 11 (2020), 241-258

987 Manchuel, K., Traversa, P., Baumont, D., Cara, M., Nayman, E., Durouchoux, C. 2018. The French
988 seismic catalogue (Fcat-17). *Bulletin of Earthquake Engineering*, 16, 2227-2251.

989 Mandier, P., 1988. Le relief de la moyenne vallée du Rhône au Tertiaire et au Quaternaire: essai de
990 synthèse paléogéographique. Documents du BRGM, 151, 217pp..

991 Mandier, P., 1989. Le relief de la moyenne vallée du Rhône au Tertiaire et au Quaternaire, essai de
992 synthèse paléogéographique. *Géocarrefour* 64, 131–132.

993 Manzi, V., Gennari, R., Hilgen, F. et al. 2013. Age refinement of the Messinian salinity crisis onset in
994 the Mediterranean. *Terra Nova*, 25(4), 315-322. <https://doi.org/https://doi.org/10.1111/ter.12038>

995 Martini, J. 2005. Etude des paléokarsts des environs de Saint-Remèze (Ardèche, France): mise en
996 évidence d'une rivière souterraine fossilisée durant la crise de salinité messinienne. *Karstologia* 45–
997 46, 1–18.

998 Martini J. 2019. Données nouvelles sur la « rivière souterraine fossile de Saint-Remèze » et ses
999 affluents: modèles spéléo-géniques et évolution morphologique régionale du Sud-Ardèche au
1000 Néogène supérieur. *Karstologia*, (74), 15-30.

1001 Martini, J. 2022. L'âge des gorges de l'Ardèche révélé par la « rivière souterraine fossile de Saint-
1002 Remèze » et données nouvelles sur les remplissages tortoniens. *Karstologia Mémoires*, 24(IV), 65-68.

1003 Masse J.P., Triat J.M., Humbert S. et al. 1980. Carte géol. France (1/50000), feuille Pont-Saint-Esprit
1004 (913). Orléans: BRGM. Notice explicative par Masse, J.P., Bois, J.J., Damiani, L., Vogt, J. (1980), 42 p.

1005 Miller, K.G., Schmelz, W.J., Browning, J.V., Kopp, R.E., Mountain, G.S., Wright, J.D. 2020. Ancient sea
1006 level as key to the future. *Oceanography* 33, 33–41. <https://doi.org/10.5670/oceanog.2020.224>

1007 Mitchum, R. M., Vail, P.R. 1977. Seismic stratigraphy and global changes of sea-level, part 7:
1008 stratigraphic interpretation of seismic reflection patterns in depositional sequences. In: Payton, C.E.
1009 (Ed.), *Seismic Stratigraphy - Applications to Hydrocarbon Exploration*. Memoir, vol. 26. American
1010 Association of Petroleum Geologists, 135-144.

1011 Mocochain, L., Clauzon, G., & Bigot, J.-Y. 2006a. The Ardèche endokarstic responses to the eustatic
1012 variations resulting from the Messinian salinity crisis. *Bull. Soc. Géol. France*, 177(1), 27-36.

1013 Mocochain, L., Clauzon, G., Bigot, J.-Y., Brunet, P. 2006b. Geodynamic evolution of the peri-
1014 Mediterranean karst during the Messinian and the Pliocene: evidence from the Ardèche and Rhône

1015 Valley systems canyons, Southern France. *Sedimentary Geology*, 188-189, 219-233.

1016 <https://doi.org/https://doi.org/10.1016/j.sedgeo.2006.03.006>

1017 Mocochain, L., Audra, P., Clauzon, G. et al. 2009. The effect of river dynamics induced by the

1018 Messinian Salinity Crisis on karst landscape and caves: Example of the Lower Ardèche river (mid

1019 Rhône valley). *Geomorphology*, 106(1), 46-61.

1020 <https://doi.org/https://doi.org/10.1016/j.geomorph.2008.09.021>

1021 Mocochain, L., Audra, P., Bigot, J.-Y. 2011. Base level rise and per ascensum model of speleogenesis

1022 (PAMS). Interpretation of deep phreatic karsts, vauclusian springs and chimney-shafts. *Bull. Soc.*

1023 *Géol. France*, 182(2), 87-93. <https://doi.org/10.2113/gssgfbull.182.2.87>

1024 Olivetti, V., Godard, V., Bellier, O. et al. 2016. Cenozoic rejuvenation events of Massif Central

1025 topography (France): Insights from cosmogenic denudation rates and river profiles. *Earth and*

1026 *Planetary Science Letters*, 444, 179-191.

1027 Pascal M., Elmi S., Busnardo R. et al. 1989. Carte géol. France (1/50000), feuille Bourg-Saint-Andéol

1028 (889). Orléans: BRGM. Notice explicative par Pascal M., Lafarge D., Chedhomme J., Glintzboeckel C.

1029 (1989), 67 p.

1030 Pictet, A., Delanoy, G., 2017. The Chabert Formation a newly defined stratigraphic unit of late early

1031 Aptian age in the southern Ardèche, SE France. *Archives des Sciences*, Genève, vol. 69, p. 3-28.

1032 Rangin, C., Le Pichon, X., Hamon, Y., Loget, N., Crespy, A.S. 2010. Gravity tectonics in the SE Basin

1033 (Provence, France) imaged from seismic reflection data. *Bull. Soc. Géol. France*, 181(6), 503-530.

1034 <https://doi.org/10.2113/gssgfbull.181.6.503>

1035 Ritz, J.-F., Baize, S., Ferry, M. et al. 2020. Surface rupture and shallow fault reactivation during the

1036 2019 Mw 4.9 Le Teil earthquake, France. *Communications Earth & Environment*, 1(1), 10.

1037 <https://doi.org/10.1038/s43247-020-0012-z>

1038 Ritz, J.-F., Baize, S., Ferry, M. et al. 2021. Analyzing the paleoseismic history of the La Rouvière fault,
1039 unexpected source of the 11-11-2019, Mw4. 9 Le Teil surface rupturing earthquake (Cévennes fault
1040 system, France). EGU General Assembly Conference Abstracts.

1041 Roveri, M., Flecker, R., Krijgsman, W. et al. 2014. The Messinian Salinity Crisis: Past and future of a
1042 great challenge for marine sciences. *Marine Geology*, 352, 25-58.
1043 <https://doi.org/https://doi.org/10.1016/j.margeo.2014.02.002>

1044 Roure S., Clauzon G., Rubino J-L., Séranne M., Camy-Peyret J., Xavier J-P. 2009. L'incision Messinienne
1045 : Cartographie des canyons du Rhône et de la Durance : Processus et implications. 12ème congrès de
1046 l'ASF, 25-31 octobre 2009, Rennes

1047 Roux J., Brulhet, J. 1997. Apport de la géophysique sismique à la connaissance de la géologie de la
1048 région de Marcoule. CNRS/Andra: Etude du Gard Rhodanien. Actes des Journées Scientifiques
1049 CNRS/Andra, Bagnols-sur-Cèze, 3, 37-61.

1050 Rubino, J.L., Lesueur, J.L., Guy, L., Clauzon, G., 1990. Le Miocène inférieur et moyen du bassin
1051 rhodanien. Stratigraphie séquentielle et sédimentologie, Publ. Spéc. Assoc. Sédim. Fr., 67 p.

1052 Sadier B. 2013. 3D et géomorphologie karstique: La grotte Chauvet et les cavités des Gorges de
1053 l'Ardèche. PhD thesis of Grenoble University, 484 p.

1054 Schlupp, A., Clauzon, G., Avouac, J-P. 2001. Mouvement post messinien sur la faille de Nîmes:
1055 implications pour la sismotectonique de la Provence. *Bull. Soc. Géol. Fr.*,172, 697-711

1056 Séranne, M., Benedicto, A., Labaum, P., Truffert, C., Pascal, G. 1995. Structural style and evolution of
1057 the Gulf of Lion Oligo-Miocene rifting: Role of the Pyrenean orogeny. *Marine and Petroleum*
1058 *geology*, 12(8), 809-820.

1059 Séranne, M., Couëffé, R., Husson, E., Baral, C., Villard, J., 2021. The transition from Pyrenean
1060 shortening to Gulf of Lion rifting in Languedoc (South France)—A tectonic-sedimentation analysis.
1061 *BSGF-Earth Sciences Bulletin*, 192(1), 27.

1062 Tassy A., Fournier F., Munch P. et al., 2014. Discovery of Messinian Canyons and new seismic
1063 stratigraphic model, Offshore Provence (SE France): Implications for the hydrographic network
1064 reconstruction. *Marine and Petroleum Geology*, 57, 25-50.

1065 Tassy, A., Villeneuve, M., Fournier, F., Borgomano, J. 2022. Géologie du canyon de Cassidaigne
1066 (Cassis, Bouches-du-Rhône). *Géologie de la France*, n°1, 1-10.

1067 Thouvenot, F., Jenatton, L., Gratier, J. P. 2009. 200-m-deep earthquake swarm in Tricastin (lower
1068 Rhône Valley, France) accounts for noisy seismicity over past centuries. *Terra Nova*, 21(3), 203-210.

1069 Urgeles, R., Camerlenghi, A., Garcia-Castellanos, D. et al. 2011. New constraints on the Messinian
1070 sealevel drawdown from 3D seismic data of the Ebro Margin, western Mediterranean. *Basin*
1071 *Research*, 23: 123-145. <https://doi.org/10.1111/j.1365-2117.2010.00477.x>

1072

1073 **FIGURE CAPTION**

1074 Figure 1: A: Synthetic structural map of the study area (black box) showing the main tectonic domains
1075 mentioned in the text and the course of the Rhône and Ardèche rivers in dotted blue lines. B:
1076 Seismotectonic map of the lower Rhône Valley between the Cévennes Fault and Nîmes Fault. Plotted
1077 historical earthquakes are from SisFrance Database (www.sisfrance.net : data from SisFrance, BRGM,
1078 EDF, IRSN, 2022), magnitudes from FCAT (Mw catalog – Manchuel et al., 2018). BDFA refers to the
1079 Potentially Active Fault Database (Jomard et al., 2017), paleoseismological works reported in (Baize et
1080 al., 2002; Bellier et al., 2021).

1081 Figure 2 : Simplified geological map of the studied area (modified from Champenois et al., 1971;
1082 Pascal et al., 1989; Masse et al., 1980; Debelmas et al., 2004) showing location of seismic profiles
1083 used in this study and the main boreholes mentioned in the text.

1084 Figure 3 : Synthetic stratigraphic log of the study area, from the Hauterivian up to Quaternary.
1085 Seismic units interpreted on seismic profiles are reported on the right side of the log.

1086 Figure 4 : Cross-correlations of the main boreholes intersecting the base of the Messinian erosional
1087 surface in the Tricastin area containing lithological data.

1088 Figure 5 : Seismic profile P4, intersecting the Rhône canyon and a tributary of the Ardèche canyon, in
1089 two-way travel time (tw) on top, and converted in depth at the bottom. The Grand Malijac borehole
1090 is projected on the depth converted seismic profile for reference. Vp velocities obtained from the
1091 depth-processing are drawn on the section for each formation. The MES is drawn in dotted red
1092 profile. See Figures 4 and 5 for stratigraphic legend and text for more details. RC: Rhône canyon;
1093 ATrC: Ardèche tributary canyon.

1094 Figure 6 : Seismic profiles P1, P2, P3 and P5 interpreted in twt. Faults are drawn in solid black
1095 profiles. The MES is drawn in dotted red line. See Figures 4 and 5 for stratigraphic legend and text for
1096 more details. PF: Pierrelatte Fault; RC: Rhône canyon; AC: Ardèche canyon; ATrC: Ardèche tributary
1097 canyon.

1098 Figure 7 : Seismic profiles P6 and P7 interpreted in twt. Faults are drawn in solid black lines. The MES
1099 is drawn in dotted red line. See Figures 4 and 5 for stratigraphic legend and text for more details. PF:
1100 Pierrelatte Fault. AC: Ardèche canyon; ATrC: Ardèche tributary canyon.

1101 Figure 8 : Seismic profiles P8D16 and P8C16 interpreted in twt. Pierrelatte and Mondragon wells are
1102 projected on the seismic profiles. Faults are drawn in solid black lines. The MES is drawn in dotted
1103 red line. See Figures 4 and 5 for stratigraphic legend and text for more details. PF: Pierrelatte Fault;
1104 RC: Rhône canyon.

1105 Figure 9 : Seismic profiles P9, P10 and 94MAR01 interpreted in twt. The MES is drawn in dotted red
1106 line. See Figures 4 and 5 for stratigraphic legend and text for more details. RC: Rhône canyon; CC:
1107 Cèze canyon; TC: Tave canyon.

1108 Figure 10: Comparison of lithologies, Gamma-Ray (GR) signals and seismic facies of the Pliocene
1109 filling units PI1 to PI4 within the Saint-Paul-Trois-Châteaux and Codolet wells. GR curves are redrawn
1110 from printed electric logs. Seismic facies SF1 to SF5 are detailed in the text.

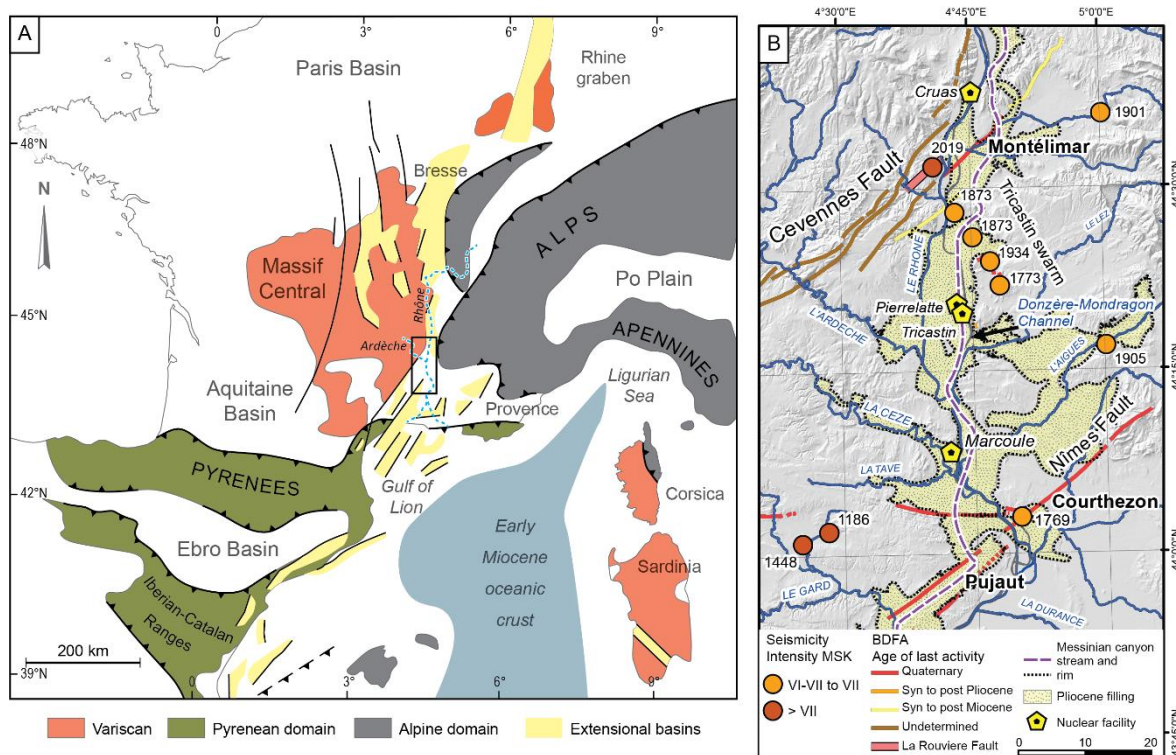
1111 Figure 11: Detailed view of the northern Mondragon anticline (seismic profile P8C16) showing the dip
1112 of Pliocene PI3 seismic unit discussed in the text. Apparent depth (left side of the figure) and
1113 apparent dip (right side of the figure) are estimated given seismic velocities retrieved from depth
1114 conversion of the P4 seismic profile (Figure 6).

1115 Figure 12: Input data (left) and resulted MES map (right) constructed by interpolating multiple
1116 parameters (current topography, depth of Pliocene basement in boreholes, depth from seismic
1117 profiles, watercourses imposed by visual analysis of seismic profiles). The topography presented is
1118 relative to sea level (hypsometry).

1119 Figure 13: Structural map showing the main structures identified on seismic profiles. Red structures
1120 are post-Cretaceous and apparently sealed by the MES. The Pierrelatte fault (PF), which has a normal
1121 component, is mechanically consistent with the regional stress field during Pyrenean orogeny if it
1122 acts as an extrados structure along the Echavarellas anticline hinge. The F3 normal fault would have
1123 behaved as a normal fault during Oligocene extension (Combes & Carbon, 1997; Ballas *et al.*, 2014) .
1124 Red structures (Mondragon frontal thrust F2 and F1) might be the only ones active during or after
1125 the Pliocene, see text for more details.

1126 Figure 1

1127



1128

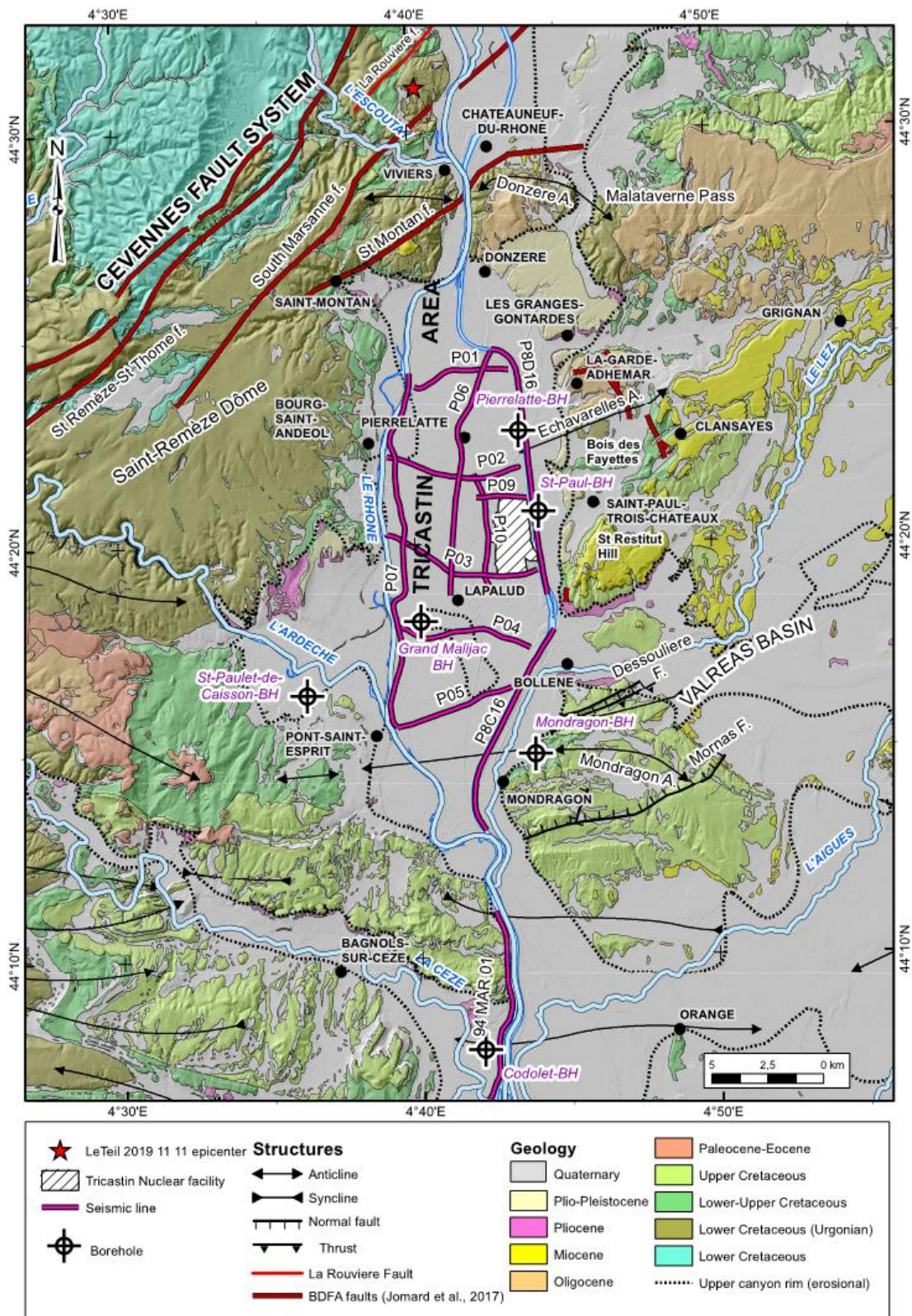
1129 A : Schéma structural synthétique de la zone d'étude (encadré noir) montrant les principaux
1130 domaines tectoniques mentionnés dans le texte et le tracé des rivières du Rhône et de l'Ardèche en
1131 pointillé bleu. B : Carte sismo-tectonique de la vallée du Rhône entre les réseaux de la faille des
1132 Cévennes et la faille de Nîmes

1133

1134 Figure 2

1135

1136

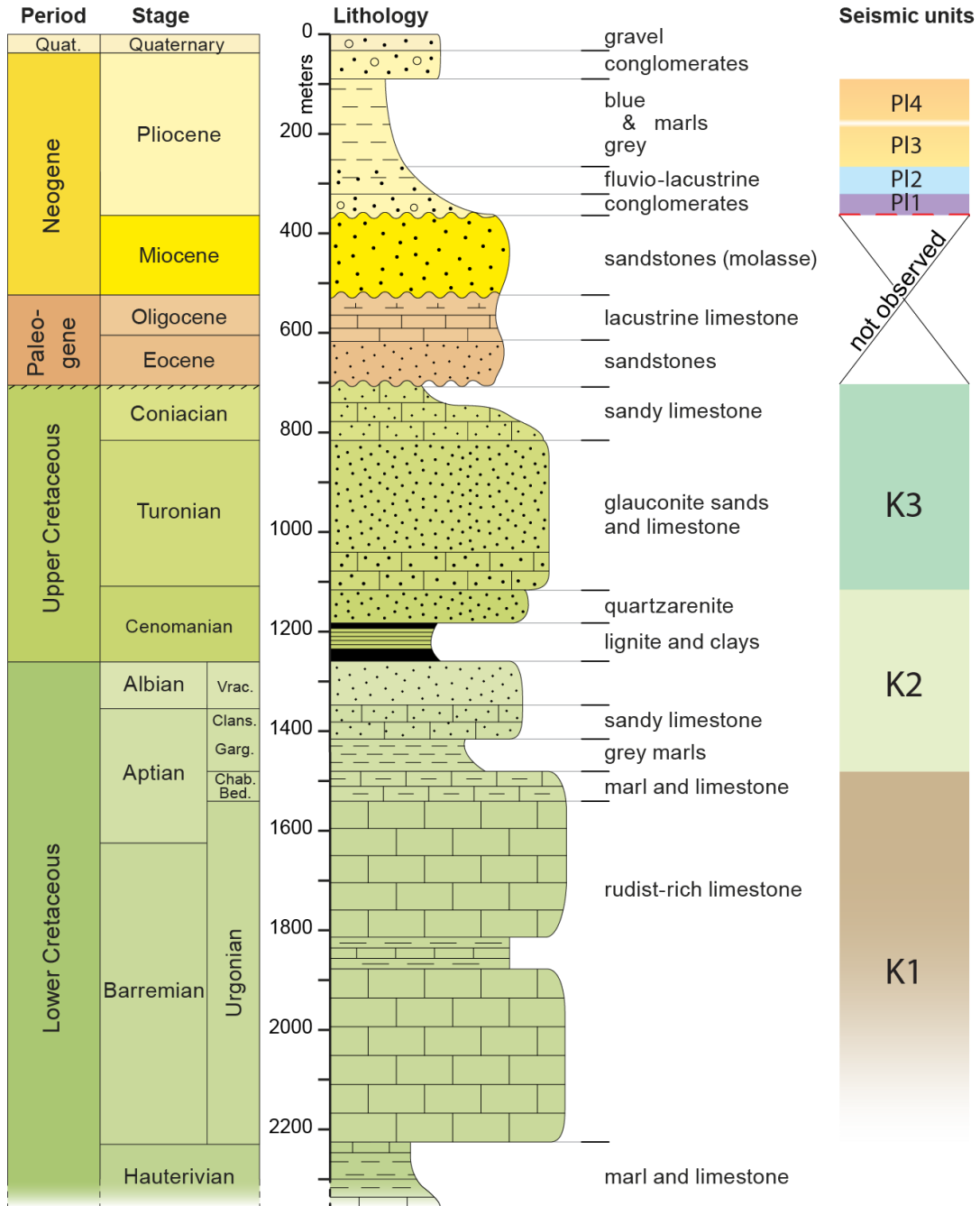


1137

1138

1139

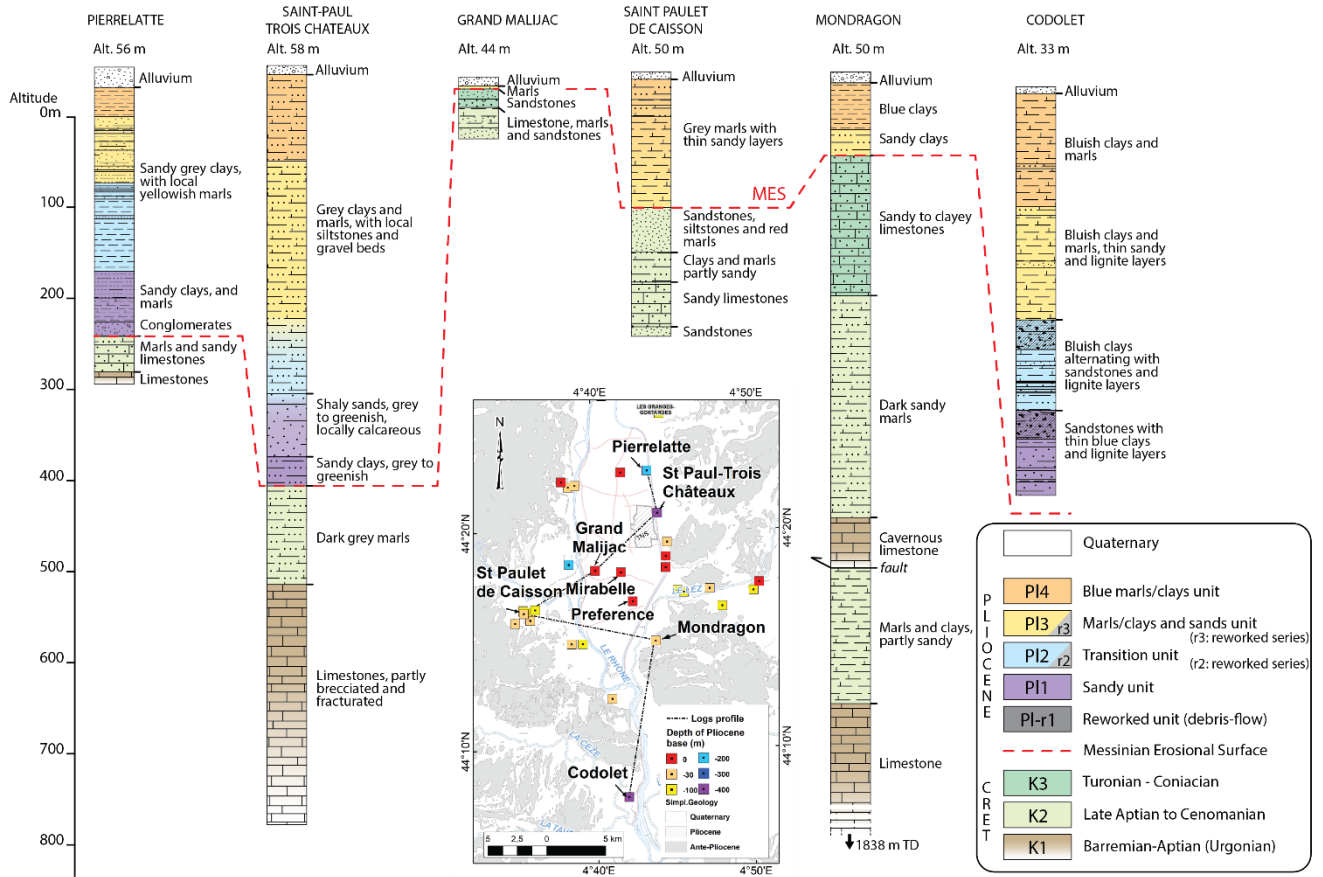
Carte géologique synthétique de la zone d'étude



1142

1143

Log stratigraphique synthétique corrélé aux unités sismiques interprétées

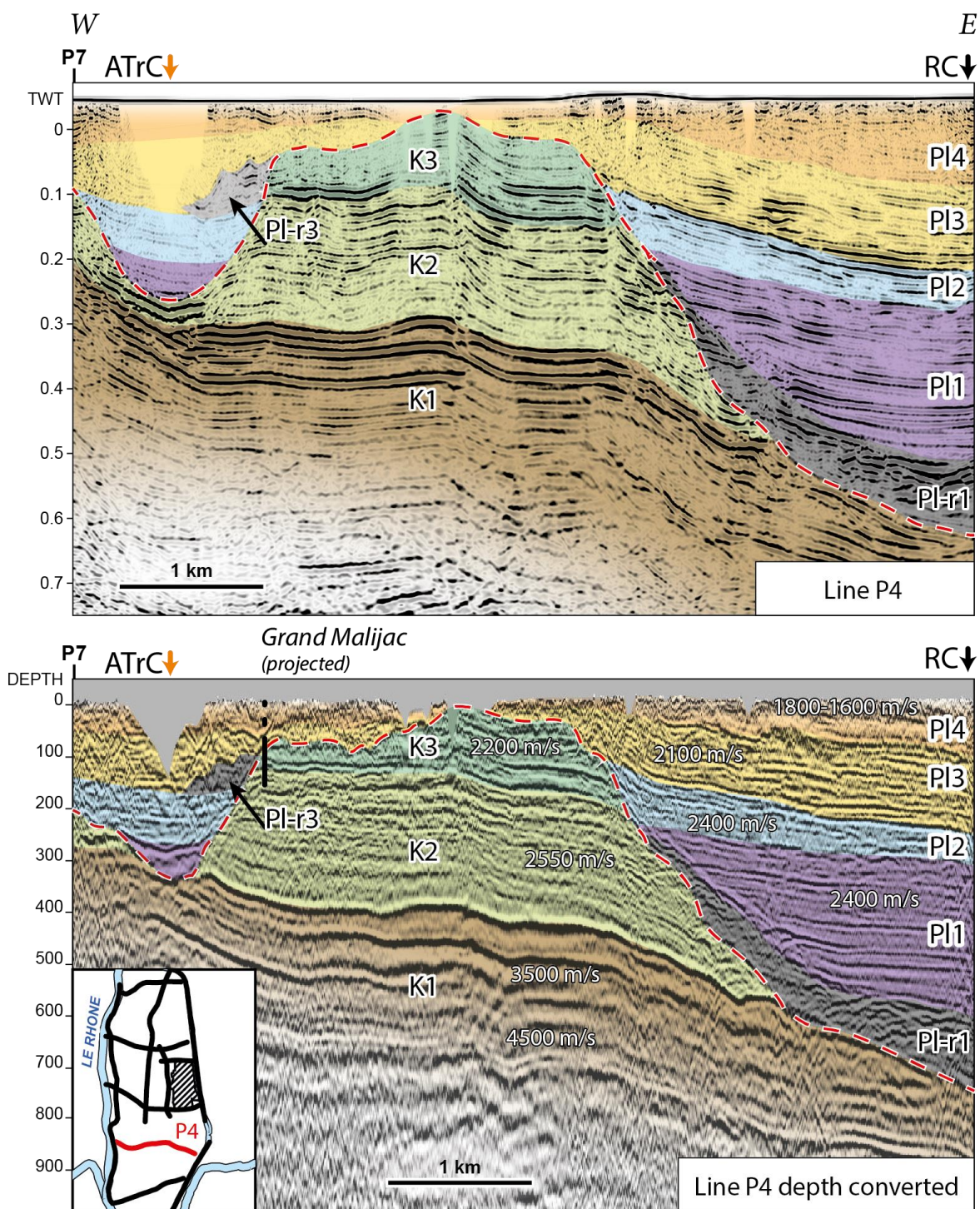


1145

1146

Corrélation stratigraphique des unités traverses par les forages profonds de la zone d'étude

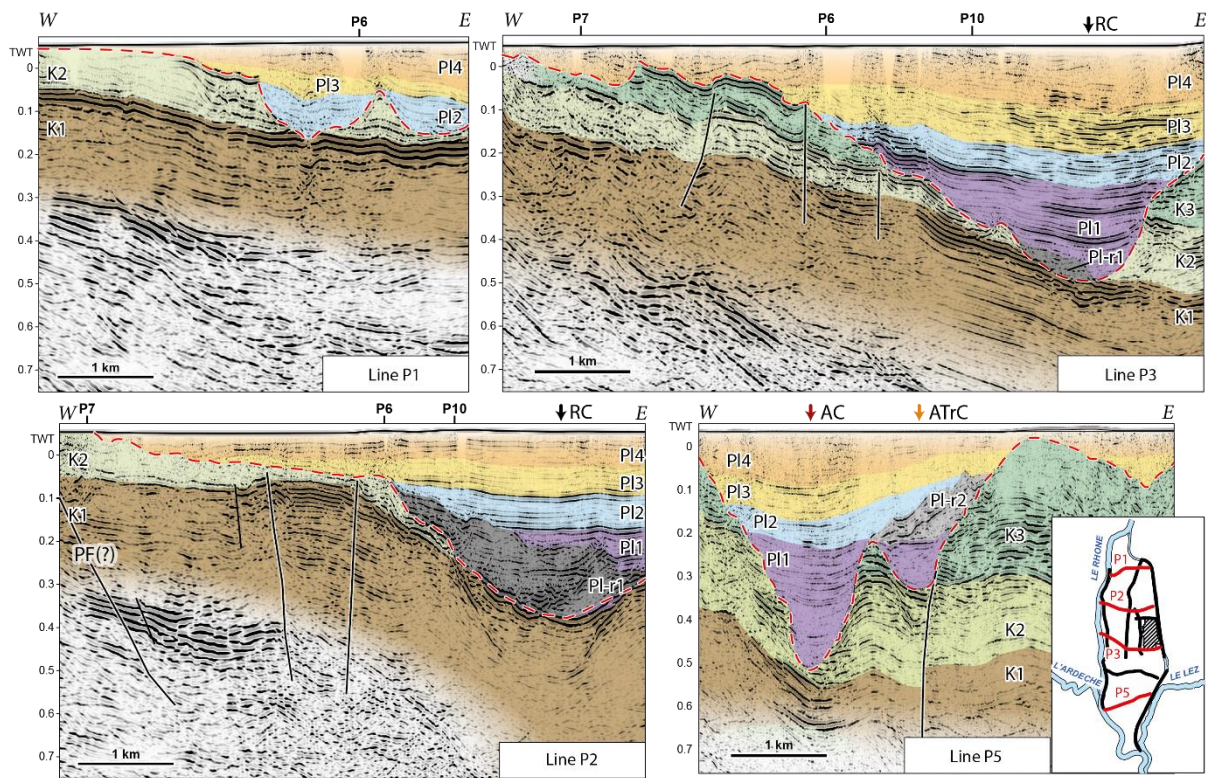
1147



1149
 1150
 1151
 1152
 1153
 1154

Profil sismique P4 interprété en temps-double et en profondeur

1155 Figure 6

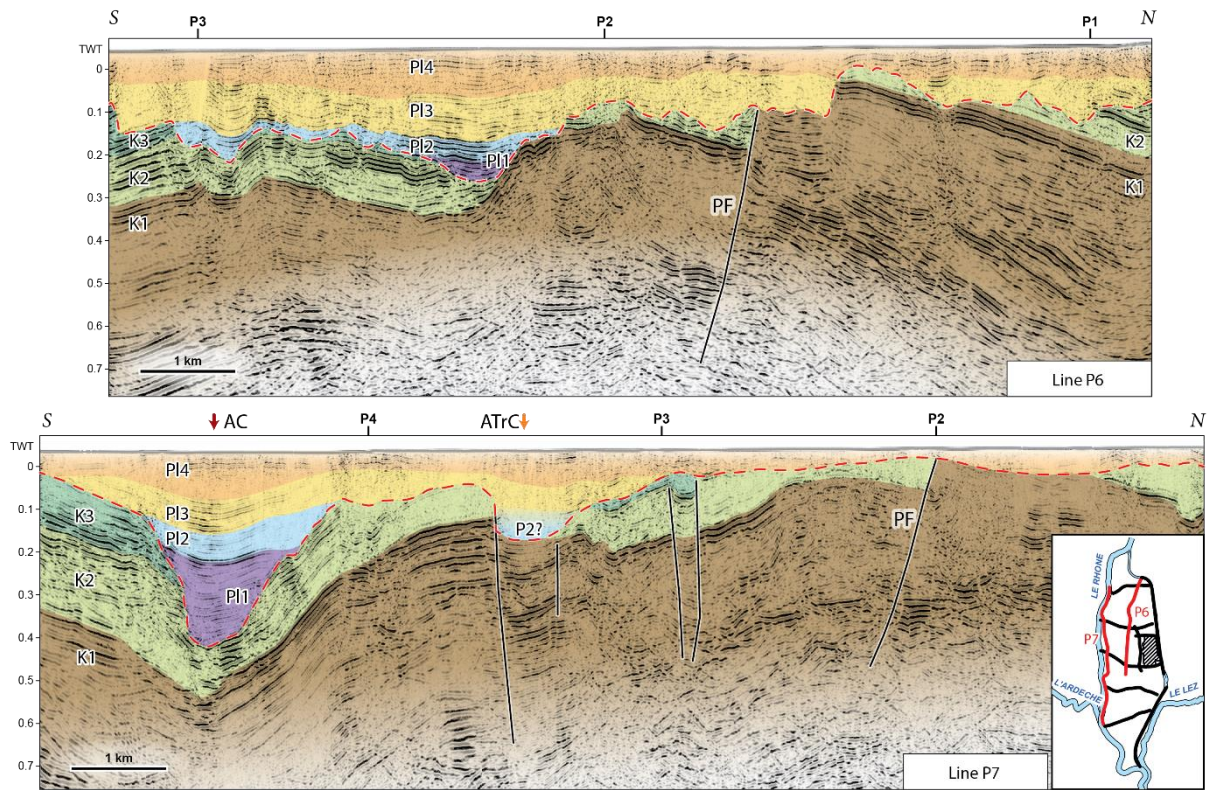


1156

1157

Profils sismique P1, P2, P3 et P5 interprétés

1158 Figure 7

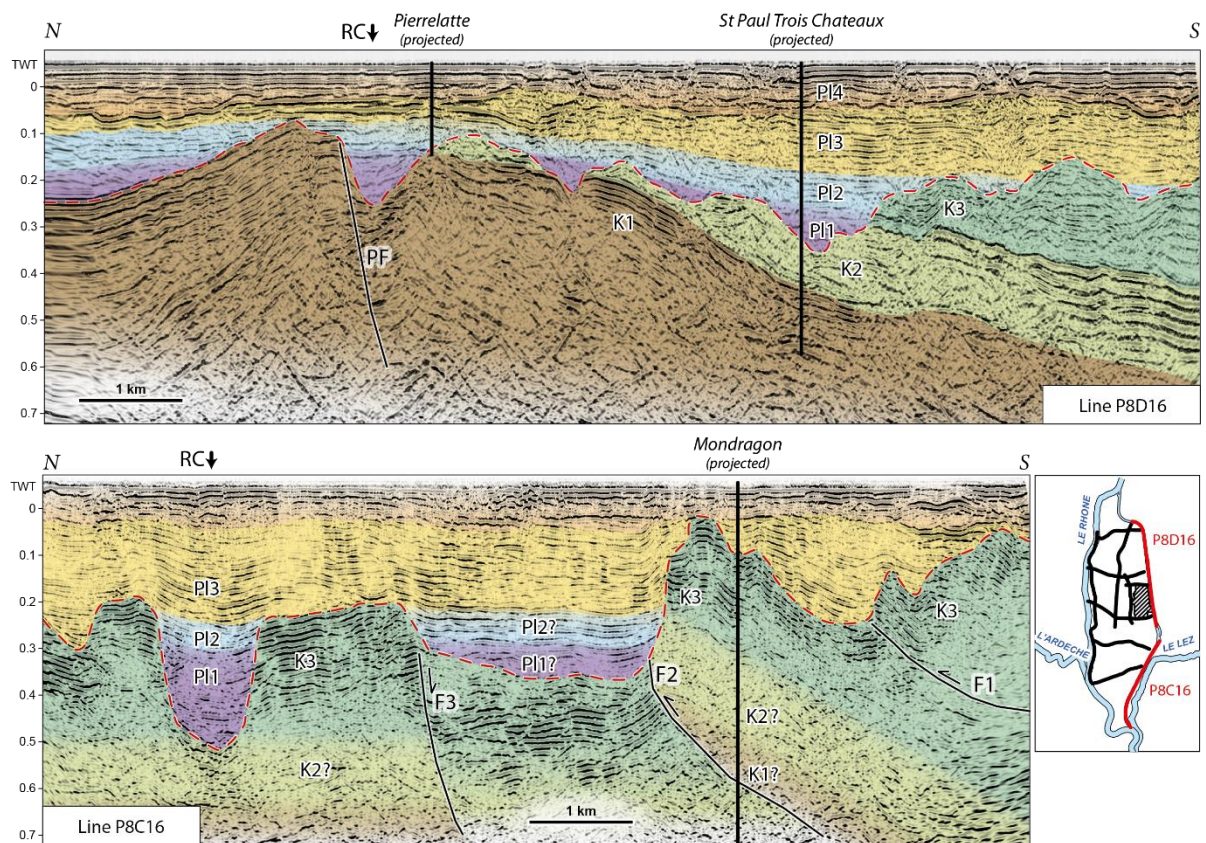


1159

1160

Profils sismique P6 et P7 interprétés

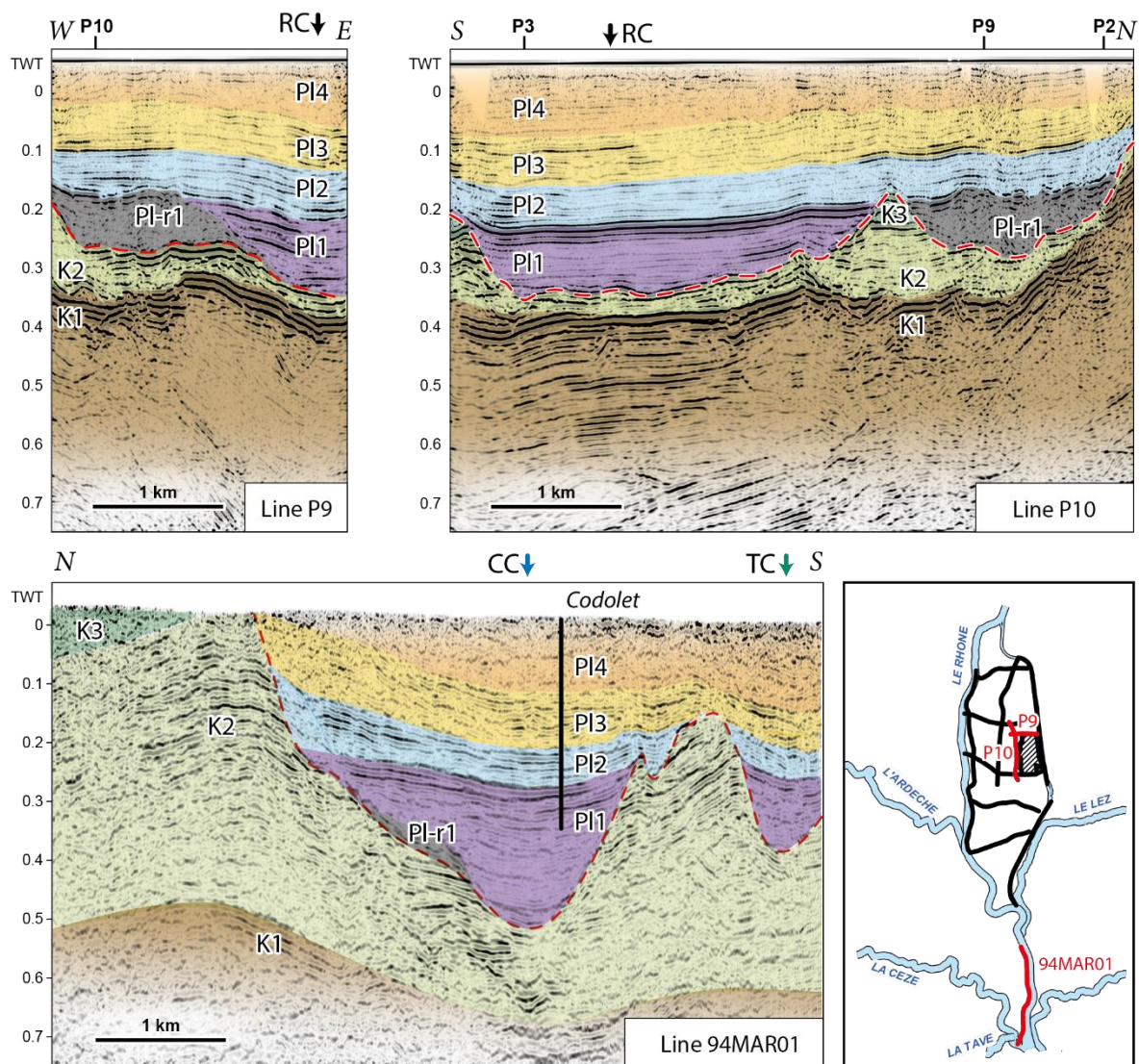
1161 Figure 8



1162

1163

Profils sismique P8D16 et P8C16 interprétés

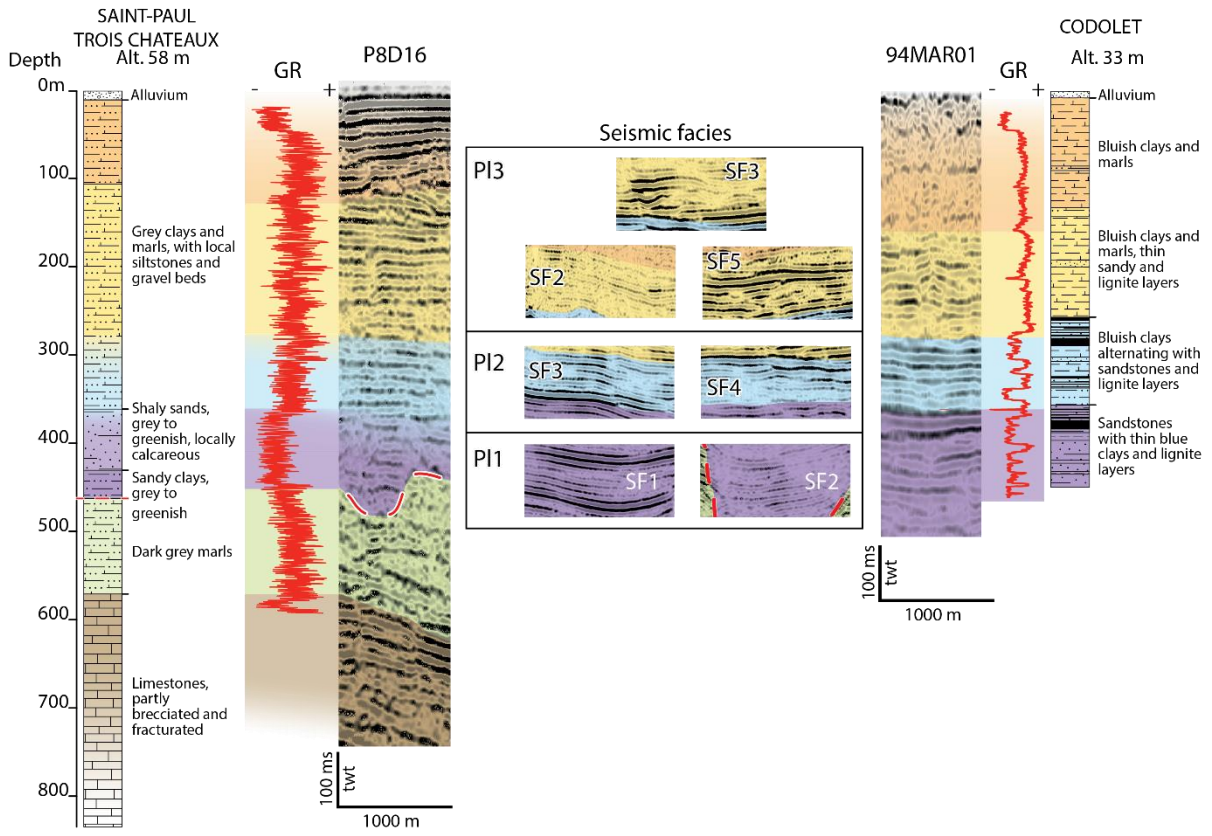


1165

1166

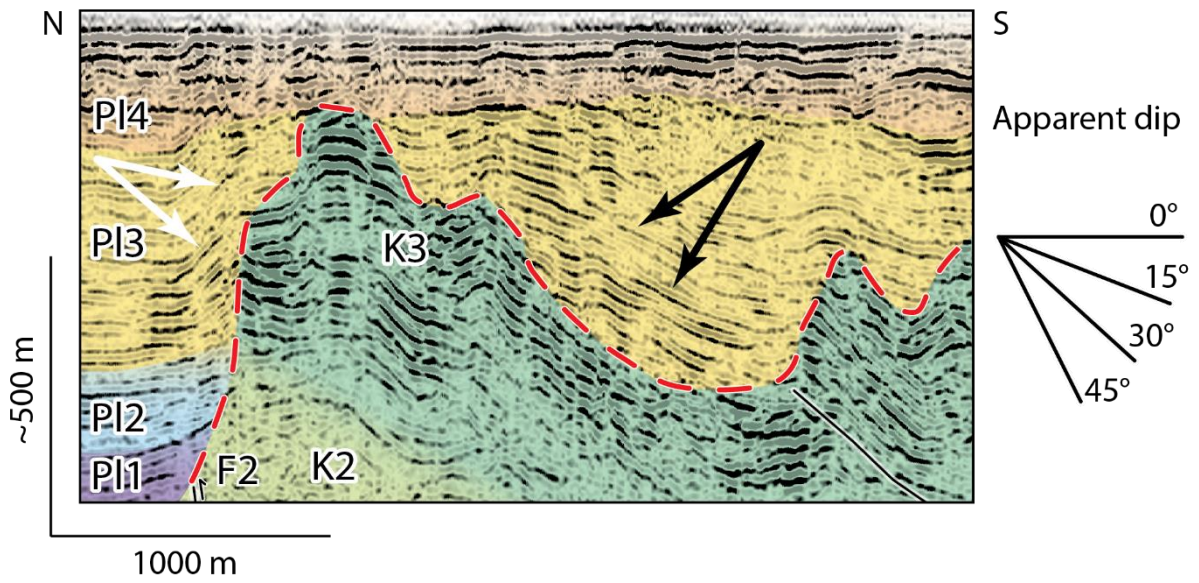
Profils sismique P9, P10 et 94MAR01 interprétés

1167 Figure 10



1168

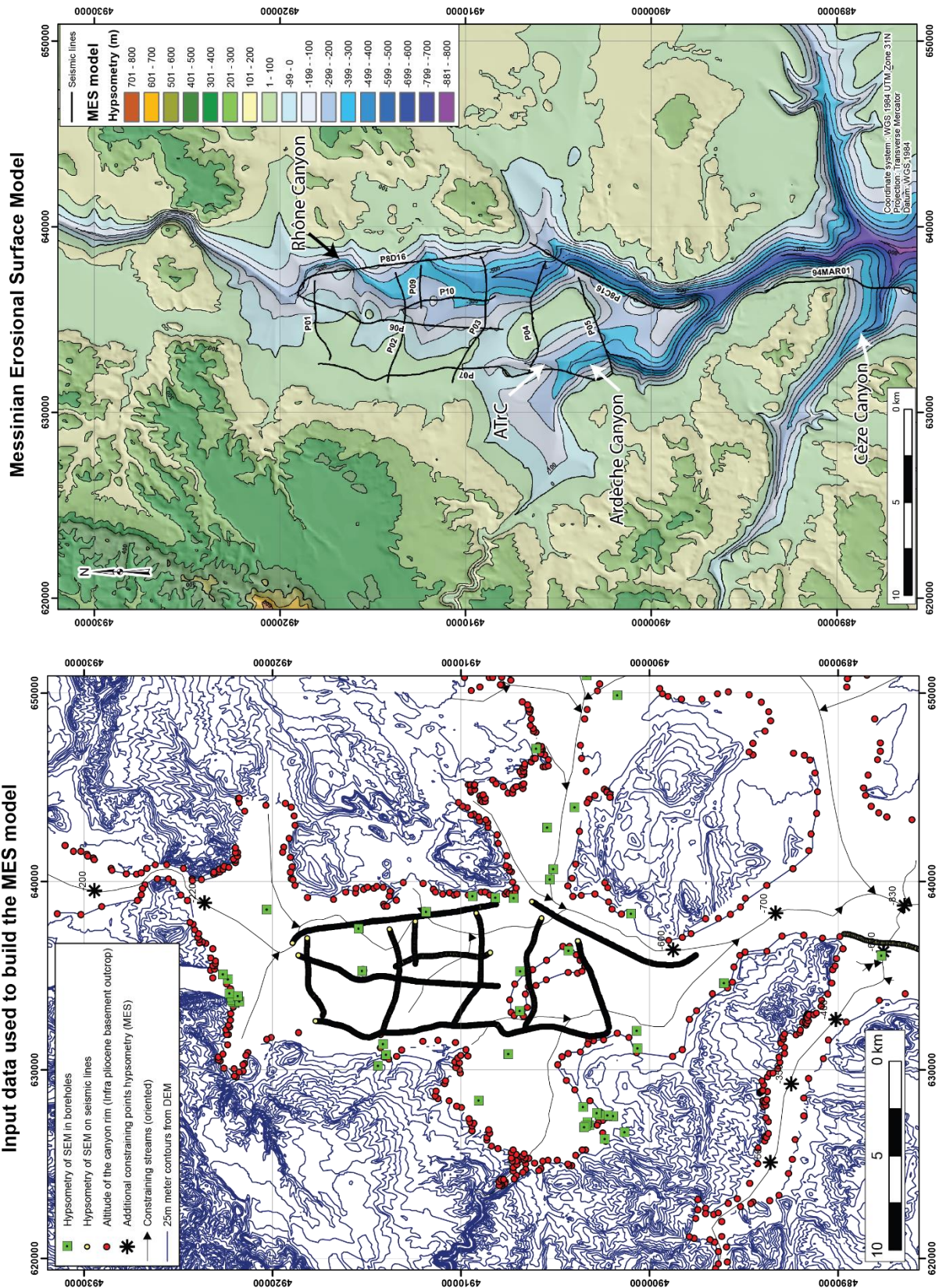
1169 Figure 11



1170

1171 Détail du profil P8C16 montrant les couches basculées dans les dépôts pliocènes de l'unit P13

1172



1174

1175

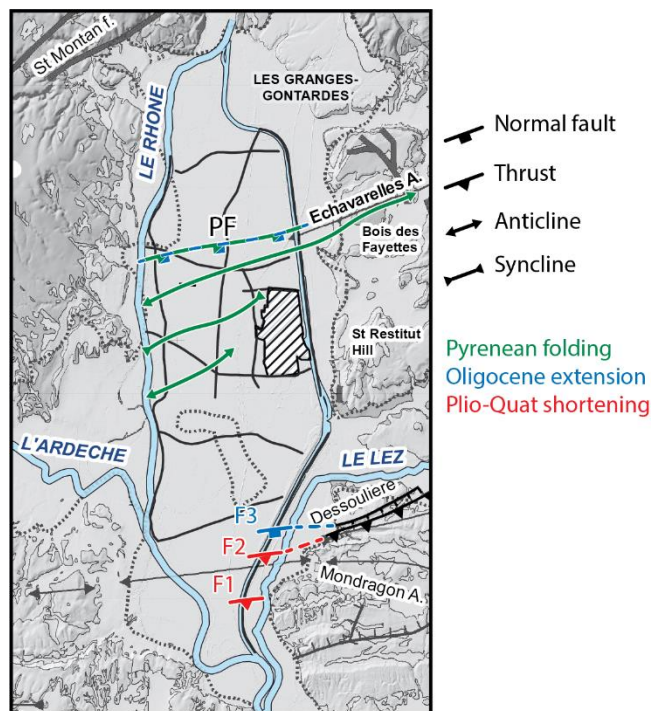
1176

1177

Carte hypsométrique de la surface d'érosion messinienne interpolée des données de surface et de profondeur Messinien

1178 Figure 13

1179



1180